HHS Public Access

Author manuscript

Nature. Author manuscript; available in PMC 2018 February 09.

Published in final edited form as:

Nature. 2017 December 07; 552(7683): 110–115. doi:10.1038/nature24676.

IL-11 is a crucial determinant of cardiovascular fibrosis

Sebastian Schafer[1,2,*], **Sivakumar Viswanathan**[2,*], **Anissa A. Widjaja**[2,*], **Wei-Wen Lim**[1], **Aida Moreno-Moral**[2], **Daniel M. DeLaughter**[3], **Benjamin Ng**[1], **Giannino Patone**[4], **Kingsley Chow**[1], **Ester Khin**[2], **Jessie Tan**[1], **Sonia P. Chothani**[2], **Lei Ye**[1], **Owen J. L. Rackham**[2], **Nicole S. J. Ko**[2], **Norliza E. Sahib**[2], **Chee Jian Pua**[1], **Nicole T. G. Zhen**[1], **Chen Xie**[1], **Mao Wang**[2], **Henrike Maatz**[4], **Shiqi Lim**[1], **Kathrin Saar**[4], **Susanne Blachut**[4], **Enrico Petretto**[2], **Sabine Schmidt**[4], **Tracy Putoczki**[5,6], **Nuno Guimarães-Camboa**[7], **Hiroko Wakimoto**[3], **Sebastiaan van Heesch**[4], **Kristmundur Sigmundsson**[2], **See L. Lim**[1], **Jia L. Soon**[1,2], **Victor T. T. Chao**[1,2], **Yeow L. Chua**[1], **Teing E. Tan**[1], **Sylvia M. Evans**[7,8,9], **Yee J. Loh**[1,10], **Muhammad H. Jamal**[1], **Kim K. Ong**[1,10], **Kim C. Chua**[1], **Boon-Hean Ong**[1], **Mathew J. Chakaramakkil**[1], **Jonathan G. Seidman**[3], **Christine E. Seidman**[3,11,12], **Norbert Hubner**[4,13,14,15], **Kenny Y. K. Sin**[1,2], and **Stuart A. Cook**[1,2,16,17]

[1]National Heart Centre Singapore, Singapore

[2]Duke–National University of Singapore Medical School, Singapore

[3]Department of Genetics, Harvard Medical School, Boston, Massachusetts 02115, USA

[4]Cardiovascular and Metabolic Sciences, Max Delbrück Center for Molecular Medicine in the Helmholtz Association (MDC), Robert-Rossle Strasse 10, 13125 Berlin, Germany

[5]Inflammation Division, Walter and Eliza Hall Institute of Medical Research, Parkville, Victoria 3052, Australia

[6]Department of Medical Biology, The University of Melbourne, Parkville, Victoria 3050, Australia

[7]Skaggs School of Pharmacy and Pharmaceutical Sciences, University of California San Diego, La Jolla, California, USA

[8]Department of Medicine, University of California at San Diego, La Jolla, California 92093, USA

Correspondence and requests for materials should be addressed to S.A.C. (stuart.cook@duke-nus.edu.sg).
*These authors contributed equally to this work.

Supplementary Information is available in the online version of the paper.

The authors declare competing financial interests: details are available in the online version of the paper.

Readers are welcome to comment on the online version of the paper.

Reviewer Information *Nature* thanks S. Friedman and the other anonymous reviewer(s) for their contribution to the peer review of this work.

Author Contributions S.A.C. conceived, managed and arranged funding for the project. Wet lab experiments (cell culture, cell biology, molecular biology, RNA-seq) were carried out by S.V., A.A.W., W.-W.L., B.N., G.P., J.T., L.Y., N.E.S., C.J.P., C.X., M.W., S.L., K.Sa., S.B., S.Schm., T.P., N.G.-C., H.W., S.v.H. and K.Si. Single-cell studies were carried out by D.M.D., J.G.S. and C.E.S. *In vivo* gain-of-function and loss-of-function mouse experiments were performed by A.A.W., W.-W.L., B.N., J.T., E.K., L.Y., N.S.J.K., N.T.G.Z., D.M.D., G.P. and H.M. Data were analysed by S.Scha., S.V., A.A.W., A.M.-M., K.C., S.P.C., O.J.L.R., K.Sa., E.P., S.M.E., J.G.S., C.E.S. and N.H. Patient-based studies were carried out by S.L.L., J.L.S., V.T.T.C., Y.L.C., T.E.T., Y.J.L., M.H.J., K.K.O., K.C.C., B.-H.O., M.J.C. and K.Y.K.S. S.Scha., S.V., A.A.W. and S.A.C. designed experiments and prepared the manuscript with input from co-authors.

[9]Department of Pharmacology, University of California at San Diego, La Jolla, California 92093, USA

[10]Kandang Kerbau Women's and Children's Hospital, Singapore

[11]Division of Cardiovascular Medicine, Brigham and Women's Hospital, Boston, Massachusettes 02115, USA

[12]Howard Hughes Medical Institute, Chevy Chase, Maryland 20815, USA

[13]DZHK (German Centre for Cardiovascular Research), partner site, Berlin, Germany

[14]Charité-Universitätsmedizin, Berlin, Germany

[15]Berlin Institute of Health (BIH), Berlin, Germany

[16]National Heart and Lung Institute, Imperial College London, London, UK

[17]MRC-London Institute of Medical Sciences, Hammersmith Hospital Campus, Du Cane Road, London, W12 0NN, UK

Abstract

Fibrosis is a common pathology in cardiovascular disease[1]. In the heart, fibrosis causes mechanical and electrical dysfunction[1,2] and in the kidney, it predicts the onset of renal failure[3]. Transforming growth factor β1 (TGFβ1) is the principal pro-fibrotic factor[4,5], but its inhibition is associated with side effects due to its pleiotropic roles[6,7]. We hypothesized that downstream effectors of TGFβ1 in fibroblasts could be attractive therapeutic targets and lack upstream toxicity. Here we show, using integrated imaging–genomics analyses of primary human fibroblasts, that upregulation of interleukin-11 (IL-11) is the dominant transcriptional response to TGFβ1 exposure and required for its pro-fibrotic effect. IL-11 and its receptor (IL11RA) are expressed specifically in fibroblasts, in which they drive non-canonical, ERK-dependent autocrine signalling that is required for fibrogenic protein synthesis. In mice, fibroblast-specific *Il11* transgene expression or Il-11 injection causes heart and kidney fibrosis and organ failure, whereas genetic deletion of *Il11ra1* protects against disease. Therefore, inhibition of IL-11 prevents fibroblast activation across organs and species in response to a range of important pro-fibrotic stimuli. These results reveal a central role of IL-11 in fibrosis and we propose that inhibition of IL-11 is a potential therapeutic strategy to treat fibrotic diseases.

Trans-differentiation of fibroblasts into activated myofibroblasts, which express α-smooth muscle actin (*ACTA2*) and secrete extracellular matrix (ECM) proteins, is a defining feature of fibrosis[8]. We automated the quantification of myofibroblasts and ECM production in primary human cardiac fibroblast cultures ($n = 84$; Extended Data Table 1 and Supplementary Table 1), and performed RNA sequencing (RNA-seq) on paired unstimulated and TGFβ1-stimulated samples (Extended Data Fig. 1). Genes were ranked on the basis of the magnitude and significance of their differential expression and their correlation with myofibroblasts. Typical fibrosis genes such as *COMP* and *NOX4*[9] were among the most-upregulated genes (Fig. 1a and Supplementary Table 2). Gene set enrichment analysis showed upregulation of genes important for protein secretion (Supplementary Table 3).

Notably, *IL11* expression showed the most positive correlation with myofibroblast numbers ($r = 0.47$, $P_{adjusted} = 6.44 \times 10^{-6}$; Spearman's correlation) (Fig. 1a) and upregulation of *IL11* expression (8.5-fold, $P_{adjusted} = 6 \times 10^{-218}$; DESeq2[10]) defined the dominant transcriptional response of cardiac fibroblasts to TGFβ1. *IL11* expression is highly specific to fibroblasts, especially when stimulated, but is undetectable in most healthy human tissues and cells[11,12] (Extended Data Fig. 2). To further explore the biological context of IL-11, we examined the expression of its receptor (*IL11RA*) compared to the receptor of IL-6 (*IL6R*), a close family member, across 512 cell lines[12]. *IL6R* was present at high levels in immune cells, whereas *IL11RA* was most highly expressed in fibroblasts (Fig. 1b).

To investigate *Il11* expression *in vivo*, we performed single-cell RNA-seq of hearts from a $Pln^{R9C/+}$ mouse, which has a cardiac fibrosis phenotype[13], and a wild-type control mouse (Fig. 1c and Extended Data Fig. 3). Both *Il11* ($P = 5.6 \times 10^{-8}$) and *Il1ra1* ($P = 2.2 \times 10^{-16}$) were enriched in fibroblasts and *Il11* was highly expressed in fibroblast subpopulations that had transcriptional features of TGFβ1 activation or ECM production (Fig. 1d). *Il11*-expressing cells were most common in fibrotic $Pln^{R9C/+}$ hearts and we confirmed Il-11 protein upregulation in this model (Extended Data Fig. 3).

IL11 has been linked to haematopoiesis[14] and tumorigenesis[15], among other roles. In contrast to a previous cardiac study[16], we found that recombinant human IL-11 (rhIL-11) is strongly pro-fibrotic in cardiac fibroblasts, increasing myofibroblasts and ECM production, motility, contraction and invasion (Fig. 1e and Extended Data Fig. 4). To better understand the apparent contradiction between our data and the previous work in which rhIL-11 was used in mouse models[16], we tested whether rhIL-11 could activate mouse cardiac fibroblasts. rhIL-11 was mostly ineffective in mouse cardiac fibroblasts, whereas recombinant mouse Il-11 (rmIl-11) activated mouse cardiac and renal fibroblasts (Extended Data Fig. 4). rhIL-11 strongly activated human renal fibroblasts.

Our findings implicate a pro-fibrotic role for IL-11 downstream of TGFβ1. In the presence of neutralizing anti-IL-11 antibodies, the pro-fibrotic effects of TGFβ1 were greatly diminished across a wide range of fibrosis assays (Fig. 1f–i and Extended Data Fig. 4). We made ligand traps by fusing IL11RA and gp130 (IL11RA:gp130) and these traps inhibited the pro-fibrotic effects of TGFβ1 in a dose- dependent manner. The specificity of IL-11 inhibition was further confirmed through inhibition of IL11RA using receptor-blocking antibodies or by short interfering RNA (siRNA), all of which attenuated the effects of TGFβ1. By contrast, anti-IL-6 antibodies had no effect on TGFβ1- induced cardiac fibroblast activation (Extended Data Fig. 4).

We next investigated the consequences of IL-11 signalling in cardiac fibroblasts using RNA-seq. Surprisingly, the effect of IL-11 on the transcriptome was negligible, whereas TGFβ1-driven transcriptional regulation in cardiac fibroblasts from the same patients remained profound (Fig. 2a, b). We repeated the experiment using cardiac fibroblasts from multiple patients and consistently observed very little effect of IL-11 on mRNA levels but, in the cell culture supernatants of identical samples, we reproducibly documented pro-fibrotic protein secretion. Therefore, the effects of IL-11 on cardiac fibroblasts are mainly at the protein

level and are unrelated to transcriptional changes (Extended Data Fig. 5). This differs from effects of IL-11 on cancer cells, in which JAK–STAT signalling is involved[17].

IL-11 can bind to free IL11RA, which is shed from cardiac fibroblast membranes (Extended Data Fig. 5) and signal *in trans* in cells that express *GP130* (also known as *IL6STP1*)[18]. We generated an IL11RA:IL-11 fusion protein (hyperIL-11), which mimics the *trans*signalling complex[19]. Concentrations of hyperIL-11 as low as 0.2 ng ml^{-1} activated cardiac fibroblasts (Extended Data Fig. 5), supporting a role for IL-11 *trans*-signalling in fibrosis.

We found that both *IL11* and *IL11RA* are expressed in fibroblasts, which implies that an autocrine signalling loop exists. Using hyperIL-11, which is not detected in an IL-11 enzyme-linked immunosorbent assay (ELISA), we confirmed the existence of autocrine IL-11 signalling in cardiac fibroblasts. This autocrine, feed-forward loop of hyperIL-11-induced IL-11 secretion is dependent on *de novo* IL-11 protein synthesis and secretion (Fig. 2c and Extended Data Fig. 5), but is independent of *IL11* RNA levels. In separate experiments, rhIL-11 (not detected by IL-11 ELISA) *cis*-signalling also strongly induced endogenous IL-11 secretion, and this also occurred in the absence of changes in *IL11* mRNA levels (Extended Data Fig. 5).

TGFβ1 activation of non-canonical ERK signalling in fibroblasts is important for fibrosis[4,5] and we observed that IL-11 also activated ERK in cardiac fibroblasts and that both TGFβ1 and IL-11 required ERK to induce pro-fibrotic phenotypes (Fig. 2d and Extended Data Fig. 5). Because the effects of IL-11 on pro-fibrotic gene expression are post-transcriptional, we suggest that this phenomenon may be driven, in part, by activation of ERK and its downstream substrates (Extended Data Fig. 5).

We therefore investigated the activation of STAT, SMAD, ERK and kinases that are important for protein synthesis in cardiac fibroblasts in response to stimulation by a range of pro-fibrotic factors. These factors included established stimuli for cardiac fibrosis (endothelin-1 (END1), angiotensin II (AngII) and PDGF) and other key pro-fibrotic cytokines (*OSM*, *bFGF*, *CTGF* and *IL13*)[1,5]. IL-11 activation of STAT in cardiac fibroblasts was negligible, consistent with its lack of transcriptional effects in this cell type. As expected, TGFβ1 activated SMAD, but the only pathway that was consistently activated by all stimuli was the ERK pathway (Fig. 2e). All pro-fibrotic stimuli that were tested induced changes in IL-11 protein levels but not mRNA; only TGFβ1 increased SMAD-dependent *IL11* transcription (Fig. 2f and Extended Data Fig. 5). Remarkably, as seen with TGFβ1, fibroblast activation in response to all pro-fibrotic stimuli that were tested was dependent on IL-11 signalling (Fig. 2g and Extended Data Fig. 6).

We studied the fibrotic response of cardiac fibroblasts from *Il11ra1*$^{-/-}$ mice[20]. TGFβ1-induced transcriptional regulation in *Il11ra1*$^{-/-}$ cardiac fibroblasts was maintained and similar to that of *Il11ra1*$^{+/+}$ (wild-type) cardiac fibroblasts ($R^2 = 0.94$, $P < 2.2 \times 10^{-16}$, Spearman's correlation; Extended Data Fig. 7). However, protein-based assays showed that cardiac fibroblasts from *Il11ra1*$^{-/-}$ mice did not increase synthesis of ECM proteins or become myofibroblasts upon stimulation (Fig. 2h and Extended Data Fig. 7), again demonstrating the effect of IL-11 at the protein level.

We investigated the role of Il-11 in a mouse model of myocardial infarction, but rather than injecting rhIL-11, as had been done in the previous study[16], we administered rmIl-11. We measured epicardial activation, a defining feature of active fibrosis in myocardial infarction[21] and found that rmIl-11 robustly stimulated fibroblasts in the epicardium (Fig. 3a–c) and caused ventricular impairment (Fig. 3d, e). We then tested the effects of rmIl-11 injection in healthy mice using regimens similar to those used for rhIL-11 in patients with cancer[22]. rmIL-11 injection in Col1a1–GFP reporter mice[23] resulted in specific activation of fibroblasts in the epicardium and renal interstitium (Fig. 3f). rmIl-11-treated mice had high circulating levels of TGFβ1, but not of other pro-inflammatory factors and features of cardiac and renal impairment along with cardiovascular fibrosis (Fig. 3g–i and Extended Data Fig. 7).

To investigate the effects of autocrine Il-11 signalling in fibroblasts *in vivo*, we generated rmIl-11-transgenic mice, which we crossed with inducible Col1a2–Cre mice (Il-11-Tg; see Methods). Il-11 was expressed after induction with tamoxifen and within two weeks, there was widespread activation of cardiac and renal fibroblasts and accumulation of collagen (Fig. 3j, k). This was accompanied by a reduction in cardiac function (Fig. 3l), increased serum TGFβ1 and an increase in serum urea and creatinine, which are biomarkers of renal failure (Extended Data Fig. 7).

Il-11 expression was found to be increased in three preclinical models of cardiovascular fibrosis (Fig. 4a, e, i). Therefore, using knockout and wild-type mice we determined whether inhibition of Il-11 could reduce fibrosis in these models. After either AngII infusion or transverse aortic constriction, less fibrosis occurred in the hearts of knockout mice compared to wild-type mice (Fig. 4b, c, f, g). This effect was independent of loading conditions (Extended Data Fig. 8). Similarly, after folateinduced kidney damage, knockout mice had reduced renal fibrosis (Fig. 4j, k). Deletion of Il11ra1 signalling resulted in reduced ERK signalling across all models tested, whereas p38 signalling was unaffected (Fig. 4d, h, l and Extended Data Fig. 9).

IL-11 was discovered owing to its ability to sustain an IL-6-dependent haematopoetic cell line when secreted from fibroblastic cells[24], but was later found to be redundant for haematopoiesis[20]. Here we show that *IL11* is a crucial fibrosis gene acting downstream of TGFβ1 and many other pro-fibrotic factors. We believe that the importance of IL-11 in fibroblasts may have gone unnoticed because its effects are apparent only at the post-transcriptional level (Extended Data Fig. 9). We highlight that *IL11RA* is not only expressed in fibroblasts but also in other cells and that IL-11 signalling may therefore be important in other cell types.

We note that rhIL-11 has been given to patients with myocardial infarction[25] and it is possible that the use of rhIL-11 in cancer patients[22] causes fibrosis-related side effects. We therefore suggest that the use of rhIL-11 in humans should be reviewed. *IL11* is highly upregulated in fibroblasts from patients with idiopathic pulmonary fibrosis or systemic sclerosis, by a 100-fold and 30-fold, respectively[26]; this suggests a role for IL-11 in fibrotic human disease beyond the cardiovascular system. IL-11 inhibitors may be particularly effective in treating fibrosis, because they would target a nodal point of pro-fibrotic

signalling. Because of these results, and target safety data from human[27] and mouse knockouts[20], we propose that IL-11 is a potential therapeutic target.

Online Content Methods, along with any additional Extended Data display items and Source Data, are available in the online version of the paper; references unique to these sections appear only in the online paper.

METHODS

Data reporting

No statistical methods were used to predetermine sample size. The experiments were not randomized.

Patient cohort

Patients ($n = 84$, aged between ≥21 and ≤81) undergoing coronary artery bypass grafting (CABG) at the National Heart Centre Singapore were recruited to the study, which was approved by the SingHealth Centralised Institutional Review Board (CIRB; 2013/103/C). Patients with valvular heart disease or previous atrial intervention were excluded. Atrial biopsies (94.6 ± 59.5 mg) were collected from the right atrium and were used to grow primary atrial fibroblasts. A summary of patient data is provided in Extended Data Table 1 and detailed patient data are presented in Supplementary Table 1.

Recombinant proteins

Commercial recombinant proteins—Human CTGF (PHG0286, Biosource), human endothelin 1 (1160/100U, Tocris), human bFGF (233-FB-025, R&D Systems), human IL-11 (PHC0115, Life Technologies), human IL-13 (PHC0134, Biosource), human oncostatin M (PHC5015, Biosource), human PDGF (220-BB-010, R&D Systems), human angiotensin II (A9525, Sigma-Aldrich), and human TGFβ1 (PHP143B, Bio-Rad).

Custom recombinant proteins—Recombinant mouse IL-11 (UniProtKB: P47873) and human IL-11 (UniProtKB: P20809) were synthesized without the signal peptide. HyperIL-11 was constructed using a fragment of IL11RA (amino acid residues 1–317 consisting of domains 1–3; UniProtKB: Q14626) and IL-11 (amino acid residues 22–199, UniProtKB: P20809) with a 20-amino-acid-long linker: GPAGQSGGGGGSGGGSGGGSV. Decoy receptors were constructed using a fragment of gp130 (amino acid residues 1–326 consisting of domains 1–3, UniProtKB: P40189) and IL11RA (amino acid residues 109–308 consisting of domains 2–3, UniProtKB: Q14626) with either a 33-amino-acid-long linker: GGGGSTRGSAGSGGSATGSGSAAGSGDSVRRGS or a 50-amino-acid-long linker: GGGGSTRGQLHTQPEVEPQVDSPAPPRPSLQPHPRLLDHRDSVEQVAVG. All custom recombinant proteins were synthesized by GenScript using a mammalian expression system.

Primary fibroblast culture

Human cardiac fibroblasts were prepared as follows: right atrial biopsies were weighed, minced into 1–2 mm^3 pieces, and placed in 6-cm dishes. Human cardiac fibroblasts were grown and maintained in DMEM (11995- 065, Gibco) supplemented with 20% fetal bovine

serum (FBS, 10500, Hyclone) and 1% penicillin–streptomycin (15140-122, Gibco), in a humidified atmosphere at 37 °C and 5% CO_2. The medium was renewed every 2–3 days. At 80–90% confluence, cells were passaged using standard trypsinization techniques. This protocol was also used to isolate fibroblasts from mouse atria, ventricles and kidneys. Human primary kidney fibroblasts (H-6016; CellBiologics) were cultured in specific medium (M2267, CellBiologics). All experiments were carried out at low cell passage (< P4) and cells were cultured in serum-free media for 16 h before treatment.

Antibodies and inhibitors used in this study were as follows: IgG type 2a (MAB003, R&D Systems), anti-IL-11 antibody (MAB218, R&D Systems), anti- IL11RA antibody (MAB1977, R&D Systems), brefeldin A (B7651, Sigma-Aldrich), cycloheximide (C1988, Sigma-Aldrich), PD98059 (9900, Cell Signaling), and U0126 (9930, Cell Signaling).

Operetta platform and image analysis

Fibroblasts were seeded in 96-well black CellCarrier plates (6005550, Perkin-Elmer) at a density of 1×10^4 cells per well. Following experimental conditions, cells were rinsed in phosphate-buffered saline (PBS) and fixed in 4% paraformaldehyde (PFA, 28908, Life Technologies). Cells were permeabilized with 0.1%Triton X-100 in PBS. EdU–AlexaFluor488 was incorporated using a Click-iT EdU labelling kit (C10350, Life Technologies) according to the manufacturer's protocol. Non-specific sites were blocked using blocking solution (0.5% BSA and 0.1% Tween-20 in PBS). Cells were incubated overnight at 4 °C with antibodies: α-smooth muscle actin (ACTA2, ab7817, Abcam), collagen I (ab292, Abcam), periostin (POSTN; ab14041, Abcam). All primary antibodies were diluted 1:500 in blocking solution. Following wash buffer (0.25% BSA and 0.1% Tween-20 in PBS) rinses, cells were incubated with the appropriate AlexaFluor488-conjugated secondary antibodies (1:1,000) for 1 h at room temperature in the dark. Cells were counter-stained with rhodamine–phalloidin (1:1,000, R415, Life Technologies) and DAPI (1 μg ml^{-1}, D1306, Life Technologies) in blocking solution. Plates were scanned and images were collected with an Operetta high-content imaging system 1483 (PerkinElmer). Each condition was assayed from at least three wells and a minimum of seven fields per well. The quantification of $ACTA2^+$ and EdU^+ cells was done using Harmony software version 3.5.2 (PerkinElmer). The measurement of collagen I and POSTN fluorescence intensity per area was performed with Columbus version 2.7.1 (PerkinElmer).

Scratch wound and migration assay

Human cardiac fibroblast migration was determined using *in vitro* scratch wound assays and Boyden chamber assays in duplicate per patient sample. Scratch wound assays were performed on confluent monolayers of fibroblasts. After synchronizing in low serum medium (DMEM containing 0.2% FBS) for 24 h, a linear scratch was created with a sterile pipette tip and cells were subjected to different treatments for 24 h. Changes in the wound area were imaged at 0 and 24 h and quantified using ImageJ software (version 1.49). Boyden chamber assays were performed using a Cell Migration Assay kit (Cell Biolabs) as per the manufacturer's protocol. Fibroblasts (5×10^4 cells per well) were seeded inside trans-well inserts, and could migrate towards the experimental conditions as in the wound assays for 24 h.

Collagen gel contraction assay

Collagen gel contraction assays were performed in duplicate per patient sample of cardiac fibroblasts (8×10^4 cells per well) using a Cell Contraction Assay kit (Cell Biolabs) as per the manufacturer's protocol. The cells were treated with stimuli similar to the scratch wound assays, except that cells were cultured in DMEM containing 1% FBS. The gels were imaged every 24 h for 72 h and gel area was quantified using ImageJ software (version 1.49).

siRNA transfection

Human cardiac fibroblasts were seeded in 96-well black CellCarrier (PerkinElmer) plates (1×10^4 cells per well) and transfected with 12.5 nM On-Targetplus siRNAs (Dharmacon) in serum-free Opti-MEM medium and DMEM containing 10% FBS (ratio 1:9) using Lipofectamine RNAiMax (13778-150, Life Technologies). The cells were transfected for 24 h and subsequently cultured in DMEM containing 1%FBS overnight before subjected to different treatment conditions.

RNA-seq library preparation

Total RNA was isolated from human cardiac fibroblasts using RNeasy columns (Qiagen). RNA was quantified using a Qubit RNA High-Sensitivity Assay kit (Life Technologies) and assessed for degradation on the basis of their RNA integrity number using the Bioanalyzer RNA 6000 Nano assay (Agilent Technologies). TruSeq Stranded mRNA Library Prep kit (Illumina) was used to assess transcript abundance following standard instructions from the manufacturer. The final libraries were quantified using KAPA library quantification kits (KAPA Biosystems) on a StepOnePlus Real-Time PCR system (Applied Biosystems) according to the manufacturer's protocol. The quality and average fragment size of the final libraries were determined using a LabChip GX DNA High Sensitivity Reagent Kit (Perkin Elmer). Libraries were pooled and sequenced on a HiSeq 2500 in High Output mode using 75-bp paired-end sequencing chemistry.

RNA-seq analysis

RNA-seq data pre-processing—Raw sequencing data (.bcl files) were demultiplexed into FastQ files with Illumina's bcl2fastq (version 1.8.4) based on unique index pairs. TopHat (version 2.0.12) was used for mapping the reads to the human genome (GRCh38.78), with the following parameters: number of threads, prefilter multihits, read mismatches, read edit distance, mate inner distance and read realign edit distance[29]. Gene level counts were computed using HTSeq[30] (version 0.6.1) with the same human genome reference used for mapping (Ensembl version 78). Ribosomal genes (Ensembl gene biotype 'rRNA') and genes located in chromosomes other than 1–22, X and Y were discarded.

Differential expression of stimulated versus non-stimulated fibroblasts—Differential expression between the stimulated and non-stimulated samples was computed at the gene level from gene counts using the DESeq2[10] R package (version 1.10.1). A pre-filtering step was used by considering only genes with counts above one across all samples (36,352 genes remained after this filter). To account for patient effects and technical artefacts, patient ID, sex and RNA concentration were added as covariates in the differential

expression model. The baseline comparison was set to non-stimulation. DESeq2 independentFiltering parameter was set to False. The rest of the parameters were left as default.

Functional enrichment of differential expression results

Gene Ontology (GO) functional enrichment of the differential expression results was performed with Gene Set Enrichment Analysis (GSEA) software (version 2.2.2). Human Ensembl genes IDs included in DESeq2[10] output were mapped gene symbols by retrieving 'hgnc_symbol' (using the biomaRt R package and Ensembl version 78). Genes without gene symbol were removed (the final number of genes was 21,412). Then all genes were ranked by the corresponding DESeq2 output Wald statistic ('stat' in DESeq2 output, defined as estimate of the $\log_2$ fold change divided by its standard error).

One functional GSEA run was performed for each GO category (BP, CC and MF) retrieved from the Molecular Signatures Database gene sets (version 5.2, gene sets queried using gene symbols)[31]. A total of three GSEA runs was carried out. GSEA was run in classic pre-rank mode with 10,000 permutations to assess the false discovery rate (FDR). In the GSEA runs, maximum cluster size was set to 5,000 and minimum cluster size was set to 10.

Computation of variation in gene expression

TPM were computed as follows. Gene read counts were divided by gene length in kilobases (gene length was computed using featureCounts software, version 1.5.1). This results in reads per kilobase (RPK). To obtain then TPM values, RPKs were divided by the sample 'per million' scaling factor (defined as the total number of gene counts in a sample divided by a million). The removeBatchEffect function from the limma R package (version 3.26.9) was used to remove technical batch effects. In removeBatchEffect, the expression matrix was set to the $\log_2(\text{TPM} + 1)$ expression matrix, the batch1 variable was set to 'library preparation batch' and the covariates variable was set to 'RNA concentration'. The obtained matrix was split into non-stimulated and stimulated. Then the removeBatchEffect function was run a second time to remove patient sex and race effects separately. From this output data, the delta of each gene was computed.

Correlation between the delta of gene expression and delta ACTA2

$ACTA2^+$ cells were measured in samples from the 84 patients as described above (Operetta image analysis). Outlier measurements were removed from the $ACTA2^+$ cells measurements. To select the measurements to be removed, we plotted the distribution of the s.d. in the measurements of each patient ($n = 3$). We removed the most distant point in the top one percentile of patients with the highest s.d. This procedure was carried out in the TGFβ1-stimulated and non- stimulated measurement separately. For each patient sample, mean ACTA2 levels were computed in baseline and stimulated fibroblasts. The corresponding delta ACTA2 was derived (defined as the difference between the mean stimulated and the mean nonstimulated). Spearman's rank correlation coefficient and the corresponding Student's *t*-test *P* value were computed between the stimulated and non-stimulated delta of each gene and the delta ACTA2 by using the function corAndPvalue from the WGCNA R package (version 1.51)[32].

RNA-seq analysis in the test cohort (patients, *n* = 9; mouse, *n* = 18)

Raw sequencing data (.bcl files) were demultiplexed into individual FastQ read files with Illumina's bcl2fastq version 2.16.0.10 on the basis of unique index pairs. The adaptor sequences and low quality reads and/or bases were trimmed using Trimmomatic version 0.36[33] and the read quality was assessed using FastQC version 0.11.5[34]. High-quality reads were mapped to Ensembl human GRCh38 version 86 reference or mouse GRCm38 version 86 reference genomes using Spliced Transcripts Alignment to a Reference (STAR) version 2.5.2b[35].

STAR alignment options were selected on the basis of the parameters used in the ENCODE project. Strand-specific raw counts of uniquely mapped (paired-end) reads were summarized with featureCounts[36] to get gene-level quantification of genomic features: featureCounts -t exon -g gene_id -s 2 –p. Differential expression was performed with DESeq2[10] version 1.14.1 using raw read counts from featureCounts. We performed a minimal pre-filtering to remove genes that have no reads or only a single read across all samples to reduce the data size and speed up the analysis process.

Sample IDs were included as covariates in DESeq2[10] design formula to remove batch effect due to samples and increase the sensitivity for finding differences among the conditions. Basal condition was always used as the reference level for pair-wise comparisons. Shrinkage MA-plot was generated to show the $\log_2$ fold changes over the mean of normalized counts and points are coloured red if the adjusted *P* value was less than 0.1.

GTEx/Fantom analysis

Two independent analyses were carried to test the tissue specificity of the expression of IL-11. These analyses used tissue expression data from the Genotype–Tissue Expression (GTEx)[11] project and the primary cell expression data from FANTOM5[12]. The test was designed to find those genes which had an expression profile that most closely matched an 'idealized' expression profile in which a gene is only expressed in stimulated fibroblasts. To do this, we used the Jennson–Shannon divergence (JSD) index, which is a measure of similarity between two probability distributions. We compared each distribution from FANTOM or GTEx incorporating our own expression data on stimulated fibroblasts to the idealized distribution. As a result, all genes with a low distance (according to JSD) to this idealized distribution are genes that are specific to stimulated fibroblasts and as such represent good candidates for further investigation.

GTEx data processing

GTEx[11] project RNA-seq V6p gene read counts (file GTEx_Analysis_v6p_RNA-seq_RNA-SeQCv1.1.8_gene_reads.gct.gz), reference annotation file (gencode.v19.genes.v6p_model.patched_contigs.gtf.gz GTEx V6p) and sample attributes (file GTEx_Data_V6_Annotations_SampleAttributesDS.txt) were downloaded from https://www.gtexportal.org/home/. TPM were computed as stated above using the downloaded gene reference annotation file. All samples provided by GTEx were used (*n* = 8,555), classified by tissue type as included in the column 'SMTS' of the sample attributes file, 30 tissues in total. Our gene TPM dataset consisting of 84 samples with unstimulated and TGFβ1-

stimulated fibroblasts was added ($n = 168$) to this GTEx data and all samples were quantile-normalized.

FANTOM data processing

Expression levels of all genes in primary cell types with replicates were downloaded from the FANTOM5 web resource (119 cell types). Because the FANTOM5 data are at the level of transcription start site expression derived from CAGE sequencing, we calculated the gene level expression by summing all counts that were assigned to a given gene. These were then normalized by library size in order to calculate the TPM for each gene. We then incorporated the TPM values from the stimulated fibroblasts and quantile normalized the data to ensure that data from the different techniques were comparable. In order to compare the expression profiles of *IL11RA* and *IL6R*, we extracted the TPM for these two genes across 511 different primary cell samples that covered cell types from all lineages. In each case, for which the expression of either *IL11RA* or *IL6R* is above the level of noise, we highlight these cell types and categorize them as described in the FANTOM5 cell type ontology.

JSD computation

On the basis of the distribution of the TPM gene expression levels in the 168 fibroblasts samples before quantile normalization, genes with average $\log_2(\text{TPM} + 1)$ higher than 2 were selected (Extended Data Fig. 2). In addition, only protein-coding genes were considered. The final number of genes included in the GTEx + fibroblasts and FANTOM + fibroblast analysis was 10,736 and 9,888, respectively.

The JSD was computed between the probability distribution of each gene and an idealized distribution, representing the situation in which a gene is only expressed in stimulated fibroblasts. The probability distribution of each gene was computed as the median gene expression in each condition, that is, GTEx tissue, FANTOM cell type or unstimulated or stimulated fibroblast, divided by the sum of the median gene expression across all conditions. The idealized probability distribution was defined as probability of 1×10^{-20} in all conditions, except for stimulated fibroblasts (with probability ~ 1). JSD was computed using the R package jsd (version 0.1).

Single-cell RNA-seq

Single-cell suspensions of non-cardiomyocytes were derived from adult left ventricles as previously described[37] either from male, 18-week-old transgenic mice[13] overexpressing $PLN^{R9C/+}$ or from FVB littermates. Single cells were isolated, lysed and subsequently RNA was reverse-transcribed and converted into cDNA libraries for RNA-seq analysis using a Chromium Controller and a Chromium Single Cell 3′ v2 Reagent kit (Genomics 10×) following the manufacturer's protocol. Libraries derived from $PLN^{R9C/+}$ or FVB mice were pooled together for DNA sequencing on a NextSeq 500 (Illumina) using a high-output kit (150 cycles) to a mean depth of > 60,000 reads per cell. Alignment of reads to the genome and generation of gene counts per cell was performed by Cell Ranger 1.2 software (Genomics 10×). Cells of sufficient complexity were clustered using *t*SNE and plots were generated using the Seurat R package[28].

Mouse models

Animal procedures were approved and conducted in accordance with the SingHealth Institutional Animal Care and Use Committee (IACUC) or in accordance with local guidelines from collaborating laboratories. All mice were from a C57BL/6 genetic background and they were bred and housed in the same room and provided food and water *ad libitum*. For *in vivo* gain-of-function studies, the mice were allocated to experimental groups to ensure equal litter/sex/age across groups. Randomization was not applicable to loss-of-function animal studies owing to genotype-dependent analyses. For gain-of-function *in vivo* studies, treatment was not disclosed to investigators generating quantitative readouts after treatment. For loss-of-function studies, genotypes were not disclosed to investigators treating the animals, or generating quantitative readouts.

Il11ra1 knockout mice

Mice lacking functional alleles for Il11ra1 (*Il11ra1*$^{-/-}$, KO) and their wild-type littermates *Il11ra1*$^{+/+}$ were 10–12 weeks of age and the weights of mice did not differ significantly. *Il11ra1*$^{+/+}$ and *Il11ra1*$^{-/-}$ male mice were subcutaneously (s.c.) implanted with an osmotic minipump (Alzet model 1004, Durect) containing either angiotensin II (AngII, 2 mg kg^{-1} per day) in saline (0.9% w/v) to stimulate cardiac fibrosis or an identical volume of saline. Mice were post-operatively treated with enrofloxacin (15 mg kg^{-1}, s.c.) and buprenorphine (0.1 mg kg^{-1}, s.c.) for three consecutive days. Kidney fibrosis was induced by intraperitoneal (i.p.) injection of folic acid (180 mg kg^{-1}) in vehicle (0.3 M $NaHCO^3$) into *Il11ra1*$^{+/+}$ and *Il11ra1*$^{-/-}$ female mice; control mice were administered vehicle alone. Mice were euthanized 28 days post-implantation or post-injection, respectively. TAC was performed in *Il11ra1*$^{+/+}$ and *Il11ra1*$^{-/-}$ male mice as described previously[38]. Post-operative treatment was performed as described above. Age-matched sham mice underwent a sham operative procedure without TAC. Trans-thoracic two-dimensional Doppler echocardiography was used to confirm increased pressure gradients (> 40 mm Hg) indicative of successful TAC. Mice were euthanized at 2 weeks post-TAC for histological and molecular assessments.

Il-11 transgenic (Il-11-Tg) model

In this model, the mouse *Il11* cDNA was expressed under the control of the ubiquitous cytomegalovirus immediate early enhancer and the chicken β-actin promoter. A *loxP*-flanked STOP cassette was introduced in between the promoter and the transgene so that overexpression could be conditionally induced by Cre recombinase. The conditional transgene was introduced into the *Rosa26* gene locus of embryonic stem cells and this transgenic mouse line is referred to here as *Rosa26-Il11* mice.

To direct transgene expression in fibroblasts, heterozygous *Rosa26-Il11* mice were crossed with *Col1a2-CreER* mice[39] to create double heterozygous *Col1a2- CreER:Rosa26-Il11* progenies (referred to here as Il-11-Tg mice). Il-11-Tg mice were injected with 1mg tamoxifen (T5648, Sigma-Aldrich) i.p. at 6 weeks of age for 10 consecutive days to induce Cre-mediated recombination. Likewise, wild-type littermates were injected with 1 mg tamoxifen for 10 consecutive days as controls.

The mice were euthanized 14 days after cessation of tamoxifen administration.

In vivo Il-11 administration model

rmIl-11 was reconstituted to a concentration of 50 μg ml^{-1} in saline. Ten-week-old male mice and transgenic *Col1a1-GFP* reporter mice[23] were subjected to daily s.c. injection with either 100 μg kg^{-1} of rmIl-11 or an identical volume of saline for 21 days.

Myocardial infarction model

Wild-type male mice (10–12 weeks) underwent myocardial infarction surgery as described previously[40]. Age-matched controls underwent sham procedures without ligation of the coronary artery. In a subset of myocardial infarction mice, rmIl-11 or an identical volume of PBS were administered daily via s.c. injection for 6 successive days.

Echocardiography

Trans-thoracic echocardiography was performed on all mice using Vevo 2100 with a MS400 linear array transducer (VisualSonics), 18–38 MHz. Mice were anaesthetized with 2% isoflurane and kept warm on a heated platform (37 °C). The chest hairs were removed using depilatory cream and a layer of acoustic coupling gel was applied to the thorax. An average of 10 cardiac cycles of standard 2D and *m*-mode short axis at mid papillary muscle level according to a previously described method were obtained and stored for subsequent offline analysis[41]. Left ventricular ejection fraction and dimensions were calculated using a modified Quinone method[42].

In vivo telemetry

Before TA11PA-C10 blood pressure device (Data Sciences International) implantation, the zero offset was measured, and the unit was soaked in 0.9% NaCl. Mice were anaesthetized with isoflurane and kept warm on a heated platform. The pressure-sensing catheter was inserted into the left carotid artery and extended into the aorta, and the transmitter was placed in a subcutaneous pocket. All mice were allowed 10 days recovery from surgery before baseline blood pressure values were recorded for five days. The data from the TA11PA-C10 device were transmitted via radio frequency signals to a receiver below the home cage and sampled every 5 min for 10 s continuously day and night with a sampling rate of 1,000 Hz. Following five days baseline pressure recording, the mice received AngII as described above. Telemetry data were collected continuously for the duration of the AngII infusion.

ELISA

The level of IL-11, IL11RA, MMP-2, and TIMP-1 in equal volumes of cell culture medium were quantified using the following kits: Human IL-11 Quantikine ELISA kit (D1100, R&D Systems), Human IL11RA ELISA kit (LSF8919, Lifespan Biosciences), Total MMP-2 Quantikine ELISA kit (MMP200, R&D Systems), Human TIMP-1 Quantikine ELISA kit (DTM100, R&D Systems). Mouse plasma level of CRP, IFNγ, TGFβ1, and TNF were measured using the following kits: CRP Quantikine ELISA kit (ab157712, Abcam), and

Mouse IFNγ ELISA kit (ab100689, Abcam), Mouse TNF ELISA kit (ab208348, Abcam), and Mouse TGFβ1 ELISA kit (ab119557, Abcam).

Colourimetric assays

Quantification of total secreted collagen in the cell culture supernatant was performed using a Sirius red collagen detection kit (9062, Chondrex). The mouse plasma levels of urea and creatinine were quantified using urea assay kit (ab83362, Abcam) and creatinine assay kit (ab65340, Abcam), respectively. The amount of total collagen in the heart and kidney was quantified on the basis of colourimetric detection of hydroxyproline using a Quickzyme Total Collagen assay kit (Quickzyme Biosciences). All colourimetric assays were performed according to the manufacturer's protocol.

RT–qPCR

Total RNA was extracted from either the snap-frozen tissues or cell lysate using Trizol reagent (Invitrogen) followed by RNeasy column (Qiagen) purification. The cDNA was prepared using an iScript cDNA synthesis kit, in which each reaction contained 1 μg of total RNA, as per the manufacturer's instructions. Quantitative RT–PCR gene expression analysis was performed on triplicate samples with either TaqMan (Applied Biosystems) or fast SYBR green (Qiagen) technology using a StepOnePlus (Applied Biosystem) over 40 cycles. Expression data were normalized to *GAPDH* mRNA expression levels and we used the $2^{-\Delta\Delta C_t}$ method to calculate the fold change. Specific TaqMan probes were obtained from Applied Biosystems and are available upon request.

Immunoblotting

Western blot analysis was carried out on total protein extracts from fibroblasts or mouse tissues. Fibroblasts or frozen tissues were homogenized by gentle rocking in lysis buffer (RIPA buffer containing protease and phosphatase inhibitors (Roche)) followed by centrifugation to clear the lysate. Equal amounts of protein lysates were separated by SDS–PAGE, transferred to a PVDF membrane, and subjected to immunoblotting analysis of p-AKT (4060, CST), AKT (4691, CST), p-EIF4E (9741, CST), EIF4E (2067, CST), p-ERK1/2 (4370, CST), ERK1/2 (4695, CST), GAPDH (2118, CST), IL-11 (MAB218, R&D Systems), p-MEK1/2 (9154, CST), MEK1/2 (4694, CST), p-mTOR (2971, CST), mTOR (2972, CST), p-p38 MAPK (4511, CST), p38 MAPK (8690, CST), p-RSK1 (11989, CST), RSK (9355, CST), p-SMAD2 (5339, CST), SMAD2 (3108, CST), p-STAT3 (4113, CST) and STAT3 (4904,CST). Proteins were visualized using the ECL detection system (Pierce) with the appropriate secondary antibodies: anti-rabbit HRP (7074, CST) and anti-mouse HRP (7076, CST). Each western blot experiment was repeated independently with similar results as follows: Fig. 2c HyperIL-11 + BFA, $n = 3$; Fig. 2e various pro-fibrotic stimuli, $n = 2$; Fig. 4a, d AngII model, $n = 5$; Fig. 4e, h TAC model, $n = 3$; Fig. 4i, l folic acid (FA) model, $n = 5$; Extended Data Fig. 3c Il-11 in PLN model, $n = 3$; Extended Data Fig. 5m HypIL-11 + BFA + CHX, $n = 2$; Extended Data Fig. 5o IL-11 time course, $n = 4$; Extended Data Fig. 5p eIF4E activation, $n = 5$; Extended Data Fig. 5q TGFβ time course, $n = 3$; Extended Data Fig. 5s various pro-fibrotic stimuli, $n = 2$; Extended Data Fig. 7n Il-11-Tg model, $n = 4$; Extended Data Fig. 9e AngII model – p38, $n = 5$; Extended Data Fig. 9f TAC model – p38, $n = 3$; Extended Data Fig. 9g FA model – p38, $n = 5$.

Histology

Tissues from TAC and Col1a1–GFP mice models were subjected to cryosectioning and tissues from all other models were paraffin-embedded. Hearts were sectioned at 5 μm and kidneys at 3 μm. For paraffin sections, tissues were fixed for 24 h, at room temperature in 10% neutral-buffered formalin (Sigma-Aldrich), dehydrated and embedded in paraffin. For cryosections, freshly dissected organs were embedded with Tissue-Tek Optimal Cutting Temperature compound (VWR International). Cryomoulds were then frozen in a metal beaker with isopentane cooled in liquid nitrogen and sections were stored in − 80 °C. Total collagen was stained with Masson's trichrome stain kit (HT15, Sigma-Aldrich) according to the manufacturer's instructions. Images of the sections were captured and blue-stained fibrotic areas were semiquantitatively determined with ImageJ software (version 1.49). For immunohistochemistry, the tissue sections were incubated with anti-ACTA2 antibody (ab5694, Abcam). Primary antibody staining was visualized using an ImmPRESS HRP Anti-Rabbit IgG Polymer Detection kit (Vector Laboratories) with ImmPACT DAB Peroxidase Substrate (Vector Laboratories) as the chromogen. The sections were then counterstained with Mayer's haematoxylin (Merck). Detection of GFP expression was performed according to established protocols[43]. Each histology experiment was repeated independently with similar results as follows: Fig. 3a myocardial infarction model, $n = 5$; Fig. 3f Col1a1–GFP model, $n = 3$; Fig. 3j Il-11-Tg model, $n = 4$; Fig. 4b AngII model, $n = 4$; Fig. 4f TAC model, $n = 3$, Fig. 4j FA model, $n = 4$; Extended Data Fig. 7i rmIL-11 model, $n = 3$.

Statistical analysis

Statistical analyses of high-content imaging, qPCR and protein data were performed using GraphPad Prism software (version 6.07). Fluorescence intensity (collagen I, POSTN) was normalized to the number of cells detected in the field and recorded for seven fields per well. Cells expressing ACTA2 were quantified and the percentage of activated fibroblasts ($ACTA2^+$) was determined for each field. Outliers (ROUT 2%, GraphPad Prism software) were removed before analysis. When several experimental groups were compared to one condition (that is, to unstimulated cells), we corrected P values according to Dunnett's. When we compared several conditions within one experiment, we corrected for multiple testing according to Sidak. The criterion for statistical significance was $P < 0.05$ ($*P < 0.05$, $**P < 0.01$, $***P < 0.001$, $****P < 0.0001$).

Data availability

High-throughput data used throughout the manuscript (Figs 1, 2, Extended Data Figs 1, 2, 5, 7 and Supplementary Information) have been deposited into the Gene Expression Omnibus (GEO; at https://www.ncbi.nlm.nih.gov/geo/) under accession number GSE97117. The authors declare that all other data supporting the findings of this study are available within the paper and its Supplementary Information. Source data are provided with the paper as Supplementary Fig. 1 (western blots) and Source Data for Figs 3, 4 (individual data points for *in vivo* studies presented in Figs 3, 4) are included in the online version of the paper. Any additional information is available upon request from the corresponding author.

Extended Data

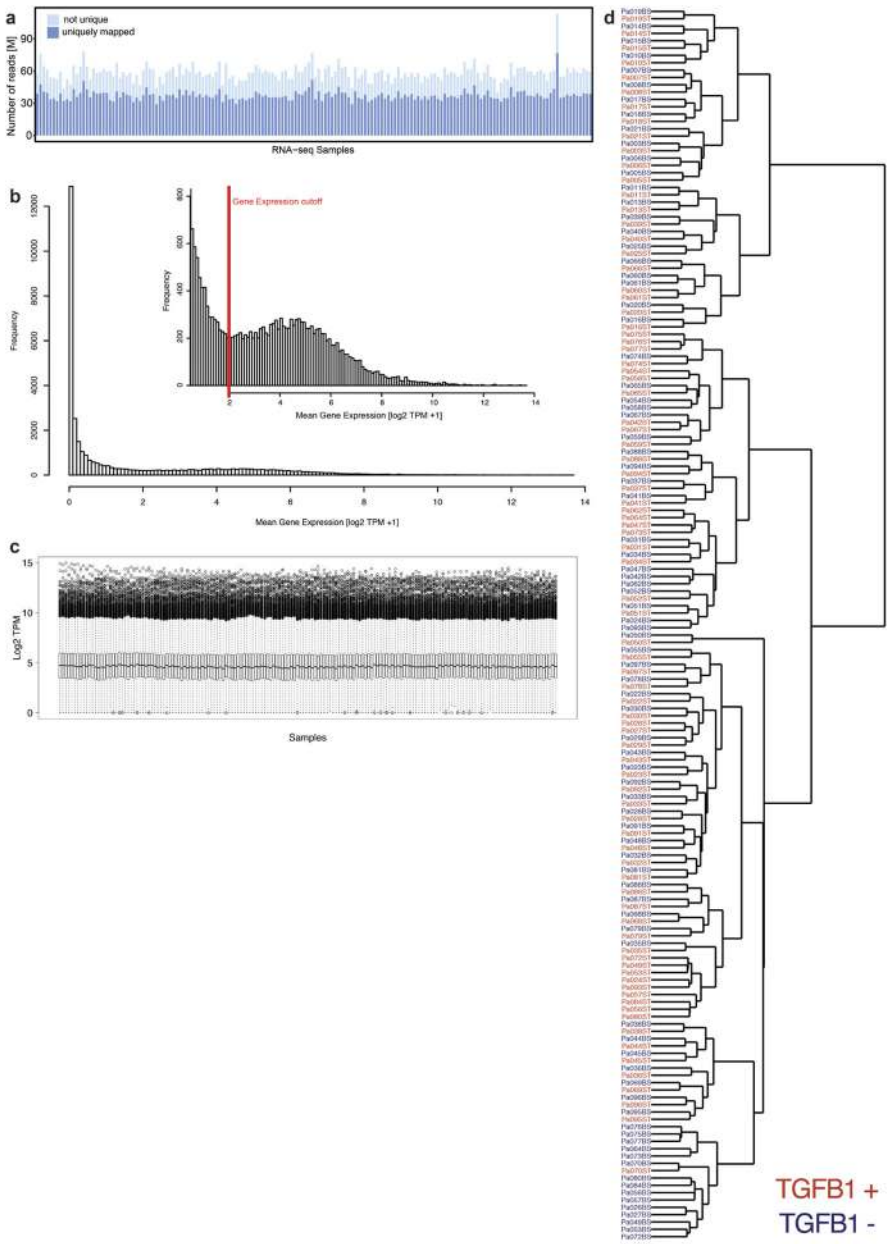

Extended Data Figure 1. RNA-seq of fibrotic cardiac fibroblasts

a, Mapped RNA-seq reads for human fibroblasts ($n = 84$ biologically independent samples). We aimed to generate at least 60 million reads per sample to assess RNA expression with and without stimulation of primary cardiac fibroblasts with TGFβ1. Fibroblasts were derived from the atria of 84 individuals, resulting in a total of 168 RNA-seq datasets for unstimulated and stimulated cells. After mapping, we used only reads that map to one unique location in the genome to estimate gene expression levels. **b**, Distribution of mean gene expression across all samples for each gene. We found 12,081 genes to be expressed at $\log_2(\text{TPM} + 1) > 2$. Genes below this cut-off were not considered in subsequent analyses. **c**,

TPM distribution for each sample after filtering ($n = 84$). **d**, Ward clustering of Euclidian distance of RNA-seq samples. Sample gene expression tends to cluster mostly by genotype, indicating a strong genetic effect, beyond the effects of TGFβ1 stimulation.

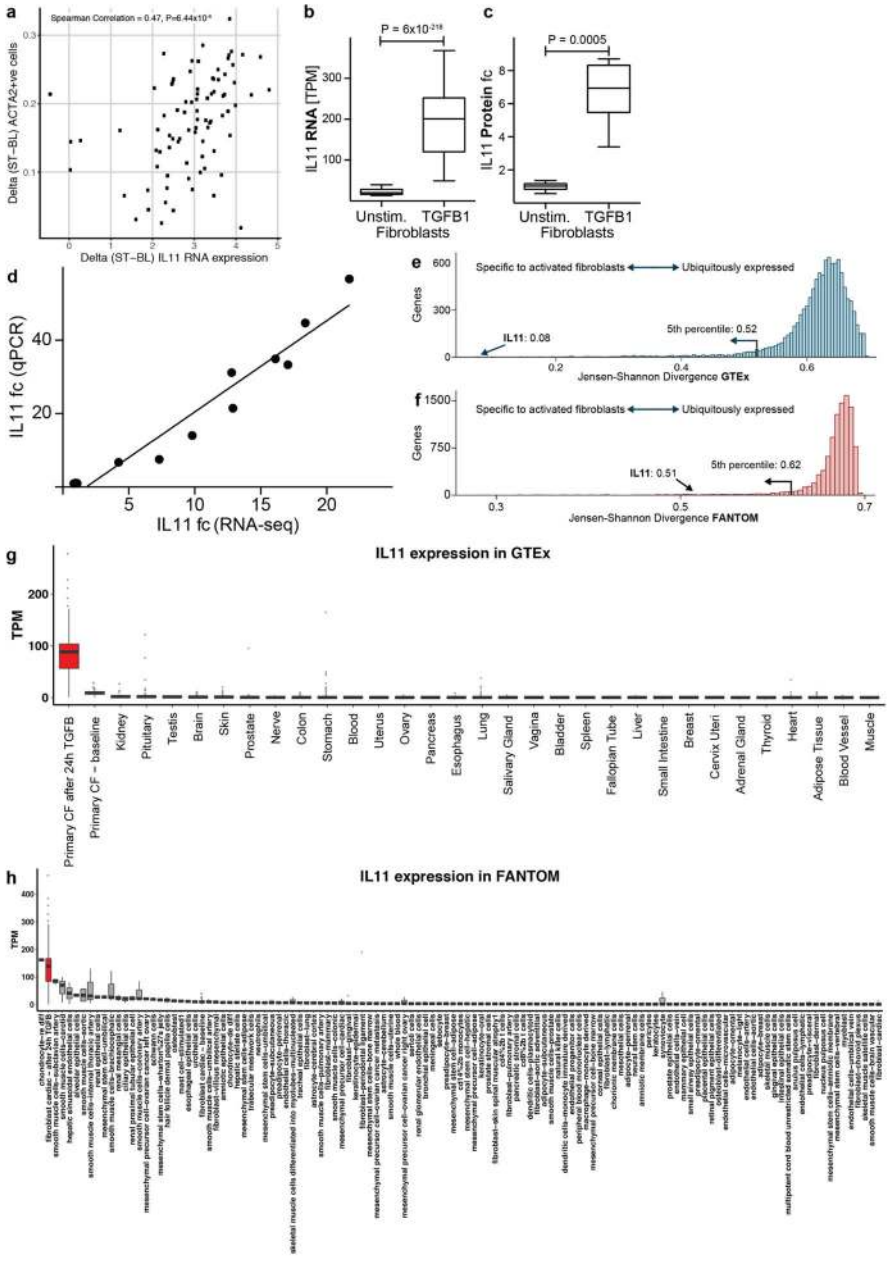

Extended Data Figure 2. Characterization the TGFβ1-regulated gene, Il-11

a, We measured the amount of activated fibroblasts ($ACTA2^+$ cells) using the Operetta High-content imaging platform and IL-11 transcript levels by RNA-seq ($n = 84$ biologically independent samples). The increase in IL-11 expression correlated strongly with fibroblast activation in the cohort ($\rho = 0.47$, 95% confidence interval = 0.28–0.62). ST, stimulated cells (5 ng ml^{-1}, 24 h); BL, baseline cells (unstimulated, 24 h). **b**, TGFβ1 (5 ng ml^{-1}, 24 h)

significantly upregulates *IL11* RNA (8.5-fold, $P = 6 \times 10^{-218}$) in human atrial fibroblasts according to RNA-seq analysis ($n = 84$ biologically independent samples). *P* values were calculated with DEseq2. **c**, The change in gene expression was confirmed at the protein level using an ELISA assay to measure IL-11 protein in the supernatant of cardiac fibroblasts ($n = 6$ biologically independent samples). fc, fold change. Two-tailed Student's *t*-test. **d**, RNA-seq-based expression differences in *IL11* transcript between unstimulated and TGFβ1-stimulated cardiac fibroblasts were confirmed via RT–qPCR. **e**, **f**, The JSD was calculated for all protein-coding genes expressed in activated fibroblasts. Low JSD scores indicate that a gene is highly expressed in stimulated cardiac fibroblasts and lowly expressed in healthy tissues (**e**; GTEx) or unstimulated, primary cell lines (**f**; FANTOM). **g**, **h**, *IL11* RNA expression in TGFβ1-stimulated and unstimulated cardiac fibroblasts ($n = 84$ biologically independent samples) compared to GTEx (**g**; tissues from $n = 8{,}723$ biologically independent samples) and FANTOM (**h**; cell types from $n = 285$ biologically independent samples) databases. **g**, RNA expression of *IL11* in TGFβ1-stimulated cardiac fibroblasts (red) and healthy tissues. **h**, RNA expression of *IL11* in TGFβ1-stimulated cardiac fibroblasts (red) and primary cells. **b**, **c**, **g**, **h**, Box-and-whisker plots show median (middle line), 25th–75th percentiles (box) and 10th–90th percentiles (whiskers).

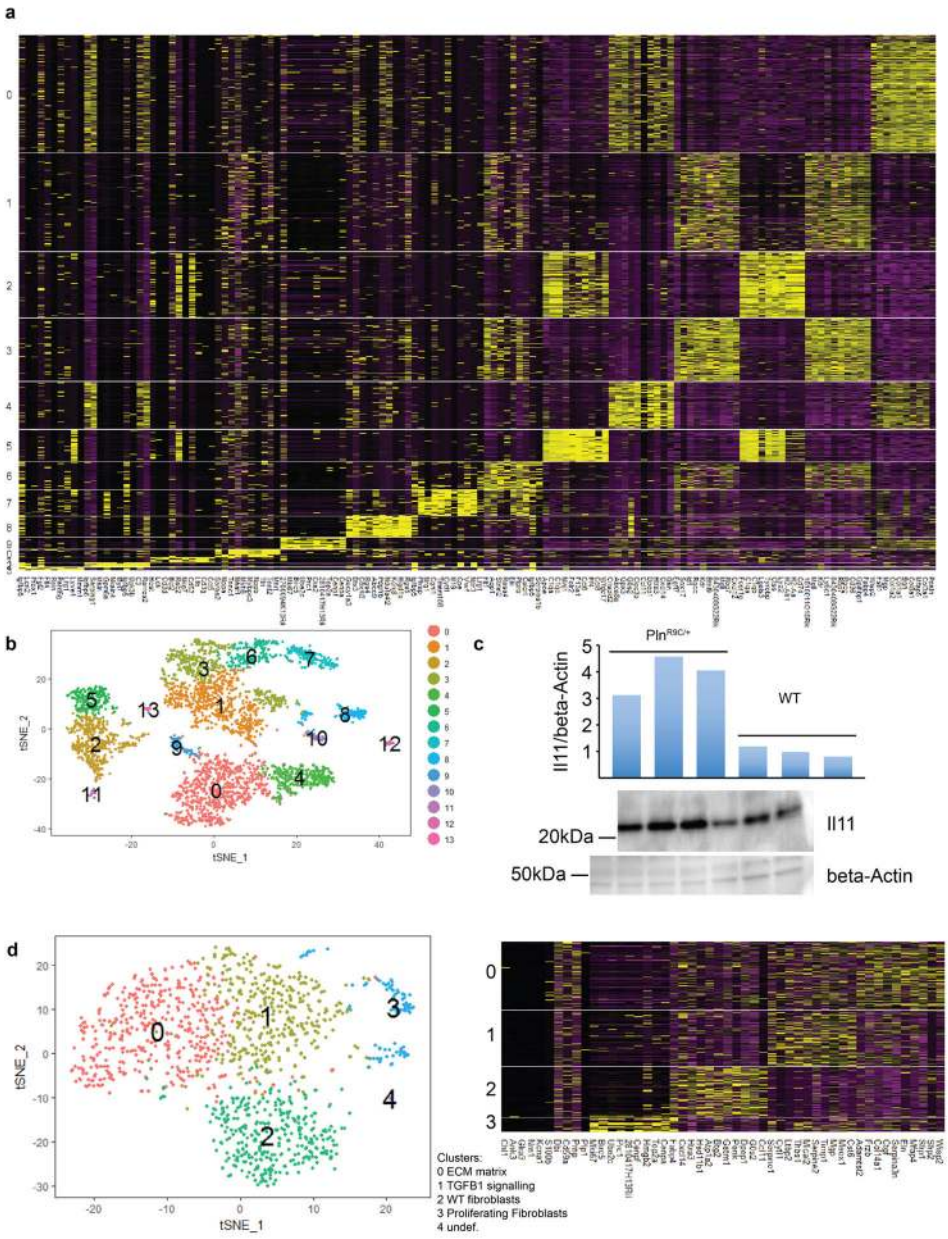

Extended Data Figure 3. Single-cell RNA-seq of fibrotic mouse heart

Single-cell RNA-seq analysis of cells isolated from $Pln^{R9C/+}$ and wild-type adult left ventricles shown in Fig. 1. **a**, Cell types were defined according to indicated marker genes. **b**, Cells were clustered and cell type was determined using the Seurat R package (see Methods). **c**, Upregulation of Il-11 in the heart in the $Pln^{R9C/+}$ fibrosis model was confirmed using western blotting. All mice were 18 weeks old and male. **d**, Subsequently, 1,263 fibroblasts from $Pln^{R9C/+}$ and wild-type mice were re-clustered using Seurat. WNT signalling, downstream of TGFβ1 in cardiac fibroblast activation, target genes were used in this analysis of the four subsequent clusters of fibroblasts; Il-11^{+} cells were primarily found in clusters 0 and 1 (16 out of 18 Il-11-expressing cells). Clusters 0 and 1 were also enriched

for $Pln^{R9C/+}$ cells compared to wild-type. Il11ra1 was expressed in all clusters. Cardiac cells were sequenced from $n = 1$ mouse, experiment was repeated one time with similar results.

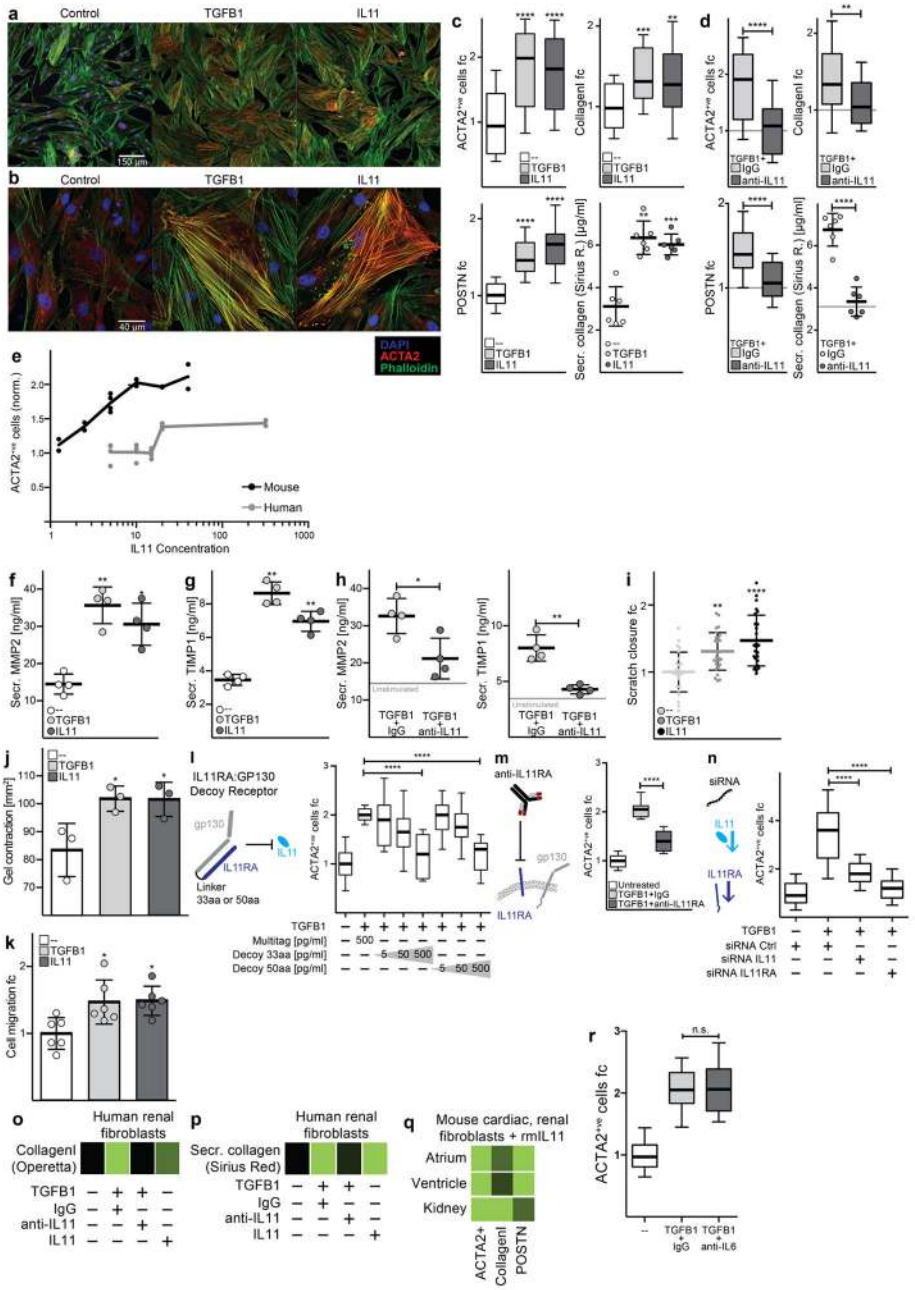

Extended Data Figure 4. IL-11 activates fibroblasts and is required for the pro-fibrotic effect of TGFβ1

a, **b**, High-resolution fluorescence imaging after TGFβ1 or IL-11 treatment (5 ng ml^{-1}, 24 h) of primary cardiac fibroblasts. Immunostaining of nuclei (DAPI, blue), ACTA2 (red) and F-actin (phalloidin, green) indicated that both TGFβ1 and IL-11 activate fibroblast stress fibre formation and increase the number of myofibroblasts *in vitro* to similar levels. Experiment was repeated four times with similar results. **c**, Automated quantification of

fluorescence (Operetta assay $n = 7$ measurements per $n = 6$ independent experiments) of primary atrial fibroblasts reveals significant fibroblast activation and ECM production induced by both TGFβ1 and IL-11 (5 ng ml^{-1}, 24 h). **d**, In addition, TGFβ1 effects can be reduced with an anti-IL-11 antibody (2 μg ml^{-1}). **c**, **d**, Collagen secretion in the supernatant ($n = 6$ independent experiments) was assessed with Sirius Red. **e**, Mouse primary fibroblasts were incubated for 24 h with indicated concentrations of recombinant human or mouse IL-11. Fibroblast activation was monitored using the Operetta High-Content Imaging platform and immunostaining for ACTA2. rhIL-11 was found to inefficiently activate mouse fibroblasts (rmIL-11, $n = 2$, rhIL-11, $n = 4$ biologically independent samples) compared to rmIL-11; this occurred for rhIL-11 treatment with rhIL-11 from two separate suppliers. **f**, **g**, MMP-2 (**f**) and TIMP-1 (**g**) concentration in the supernatant (ELISA) of cardiac fibroblasts ($n = 4$ biologically independent samples) without stimulus (–), with TGFβ1 or IL-11 (5 ng ml^{-1}, 24 h). **h**, Il-11-neutralizing antibodies (anti-IL-11, 2 μg ml^{-1}) block the increase in MMP-2 and TIMP-1 protein. **i**, *In vitro* monolayer scratch wound assay of cardiac fibroblasts. Wound closure was compared between stimulated (TGFβ1 or IL-11; 5 ng ml^{-1}, 24 h) and unstimulated cardiac fibroblasts ($n = 5$ biologically independent samples) after 24 h. **j**, Cardiac fibroblasts ($n = 3$ biologically independent samples) were seeded in collagen gel and the contraction was monitored. The area of contraction is compared between stimulated (TGFβ1 or IL-11; 5 ng ml^{-1}) and unstimulated groups after 72 h. **k**, Trans-well migration assay. After 24 h of stimulation (TGFβ1 or IL-11; 5 ng ml^{-1}), cardiac fibroblasts ($n = 6$ biologically independent samples) that crossed the membrane towards either a TGFβ1- or IL-11-containing compartment were colourimetrically quantified and compared to data from unstimulated cells. **l**–**n**, Cardiac fibroblasts were incubated with TGFβ1 (5 ng ml^{-1}, 24 h) and indicated amounts of IL11RA:gp130 decoy receptors (**l**; 33 amino acid (aa) or 50 aa linker peptide), anti-IL11RA antibody (**m**; 2 μg ml^{-1}) or siRNA pools against IL-11 or IL11RA (**n**). **l**–**n**, Fibroblast activation was monitored via immunostaining for ACTA2 on the Operetta platform. decoy receptors (**l**): $n = 7$ measurements per $n = 2$ independent experiments; anti- IL11RA (**m**): $n = 7$ measurements per $n = 2$ independent experiments; siRNA (**n**): Operetta assay $n = 7$ measurements per $n = 10$ independent experiments. **o**, Human renal fibroblasts were incubated with TGFβ1 or IL-11 (5 ng ml^{-1}, 24 h) in the presence or absence of anti-IL-11 or an IgG control antibodies (2 μg ml^{-1} each) for 24 h. ECM was assessed using the Operetta platform by staining for collagen I. Fluorescence was normalized to non-stimulated cells (black). **p**, These results were confirmed with Sirius red assay of the total collagen in the supernatant. **q**, rmIl-11 stimulation (5 ng ml^{-1}, 24 h) also activated mouse cardiac and renal fibroblasts. Myofibroblasts and ECM were assessed using the Operetta platform by staining for ACTA2, collagen I or POSTN. Fluorescence was normalized to non-stimulated cells (black). **o**–**q**, These experiments were repeated three times with similar results. **r**, Cardiac fibroblasts analysed on the Operetta high-content imaging platform with immunostaining of ACTA2 after 24 h incubation without stimulus, TGFβ1 (5 ng ml^{-1}, 24h) or TGFβ1 and IL-6-neutralizing antibody (2 μg ml^{-1}, 24h). Automated quantification of fluorescence (Operetta assay $n = 7$ measurements per $n = 6$ independent experiments) shows no significant decrease in fibroblast activation using anti-IL-6 antibodies. Data are mean and circles show individual values (**e**) or mean ± s.d. and circles show individual values (**c, d** bottom right, **f**–**h**, **k**); box-and-whisker plots (**c**, **d**, **l**–**n**, **r**) show median (middle line), 25th–75th percentiles (box) and 10th–90th percentiles

(whiskers). Two-tailed Dunnett's test (**c**, **f**, **g**, **i**–**k**), two-tailed Student's *t*-test (**d**, **h**, **r**) or two-tailed, Sidak-corrected Student's *t*-test (**l**–**n**). **P* < 0.05; ***P* < 0.01; ****P* < 0.001; *****P* < 0.0001.

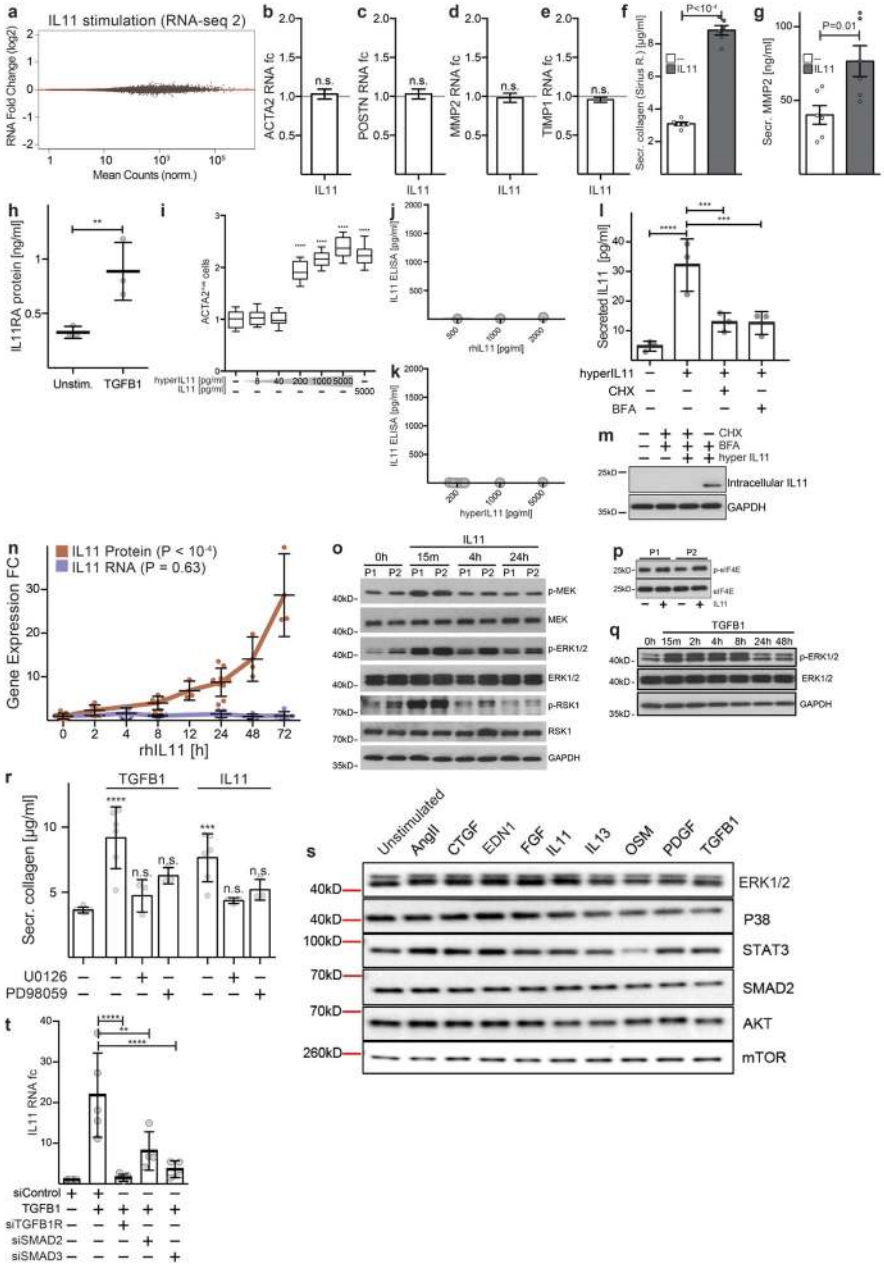

Extended Data Figure 5. IL-11 drives fibrogenic protein expression via non-canonical ERK signalling

a, Genome-wide RNA expression differences of cardiac fibroblasts in response to IL-11 (*n* = 4 biologically independent samples, 5 ng ml^{-1}, 24 h). Red indicates differentially expressed genes according to DEseq2. Fibrosis gene RNA is not increased by IL-11 treatment. **b**–**e**, RT–qPCR experiments for RNA expression of *ACTA2* (**b**), *POSTN* (**c**), *MMP2* (**d**) and

TIMP1 (**e**) in response to IL-11 treatment (5 ng ml^{-1}, 24 h) compared to unstimulated cells. IL-11 does not significantly upregulate these genes at the RNA level in cardiac fibroblasts (n = 4 biologically independent samples). **f**, Sirius red assay reveals significant increase in collagen protein. **g**, ELISA reveals increase in MMP-2 protein in the supernatant of the samples (shown in Fig. 2b, n = 6 biologically independent samples) that lack a change in RNA transcripts. **h**, Concentration of IL11RA (ELISA) in the supernatant of cardiac fibroblasts (n = 3 biologically independent samples) after TGFβ1 stimulation (5 ng ml^{-1}, 24 h). **i**, Cardiac fibroblasts were incubated with increasing concentrations of a fusion protein consisting of IL-11 and IL11RA connected with a linker peptide that recapitulates the features of the IL-11 *trans*-signalling complex. Concentrations as low as 200 pg ml^{-1} significantly activated cardiac fibroblasts as measured using a highcontent imaging platform and staining for ACTA2 expression (Operetta assay n = 7 measurements per n = 4 independent experiments). **j**, **k**, rhIL-11 (**j**) and hyperIL-11 (**k**) were added at indicated concentrations and subsequently measured using a commercially available IL-11 ELISA (n = 1 independent experiment). The ELISA did not detect rhIL-11 or hyperIL-11. We note that the reactivity to rhIL-11 was variable dependent on batch and provider and rhIL-11 was sometimes detected. However, in all experiments presented in the main figures, we confirmed that the rhIL-11 used was not detectable by the ELISA by additional measurements. This ELISA reliably detected native IL-11 secreted by human fibroblasts. **l**, Cardiac fibroblasts (n = 3 biologically independent samples) were incubated (8 h) with hyperIL-11 (0.2 ng ml^{-1}) in the presence of absence of the inhibitor of protein translation, cyclohexamide (CHX, 5 μg ml^{-1}), or protein secretion, brefeldin A (BFA, 1 μg ml^{-1}). Both inhibitors block the increase in IL-11 protein in the supernatant in response to hyperIL-11 treatment. **m**, Western blot and ELISA of IL-11 in cardiac fibroblasts after hyperIL-11, the inhibitor of the Golgi secretory pathway BFA and/or the translation inhibitor CHX treatment shows *de novo* protein synthesis and canonical secretion of IL-11 after stimulation. **n**, ELISA (n = 9 biologically independent samples) and RT–qPCR (n = 5 biologically independent samples) assays show an increase in endogenous IL-11 protein but not RNA over time after rhIL-11 (5 ng ml^{-1}) treatment. **o**, ERK signalling pathway activation by TGFβ1 and IL-11. Western blots show activation of the non-canonical MEK–ERK– RSK cascade in response to IL-11 stimulation of human cardiac fibroblasts. Here the response was greatest at 15 min in the two patients analysed, but more prolonged ERK activation was also seen in additional experiments. **p**, Downstream substrates of ERK, such as eIF4E, were also phosphorylated by rhIL-11. **q**, TGFβ1 also activates the ERK pathway. The time course and degree of activation was variable between patients. **r**, Collagen secretion (Sirius red) from cardiac fibroblasts (control, n = 6; TGFβ1, n = 6; TGFβ1 + U0126, n = 3; TGFβ1 + PD98059, n = 3; IL-11, n = 6; IL-11 + U0126, n = 3; IL-11 + PD98059, n = 3 biologically independent samples) induced by TGFβ1 or IL-11 (5 ng ml^{-1}, 24 h) is reduced by two separate MEK inhibitors (10 μM). **s**, Western blot of total protein levels of key signalling molecules in fibroblasts after 24 h stimulation with AngII (100 nM), CTGF (50 ng ml^{-1}), EDN1 (250 ng ml^{-1}), bFGF (10 ng ml^{-1}), IL-13 (100 ng ml^{-1}), OSM (100 ng ml^{-1}), PDGF (200 ng ml^{-1}) and TGFβ1 (5 ng ml^{-1}). The corresponding activated protein levels are shown in Fig. 2e. **t**, siRNA treatment of TGFβ1-stimulated cardiac fibroblasts. RT–qPCR shows SMAD-dependent upregulation of *IL11* RNA (control, n = 8; TGFβ1, n = 5; si*TGFB1R*, n = 5; si*SMAD2*, n = 4; si*SMAD3*, n = 4 biologically independent samples). Data are mean ±

s.d. (**b**–**h**, **l**, **n**, **r**, **t**); box-and-whisker plots (**i**) show median (middle line), 25th–75th percentiles (box) and 10th–90th percentiles (whiskers). Two-tailed Student's *t*-test (**b**–**h**), two-tailed Dunnett's test (**i**, **r**) or Sidak-corrected, two-tailed Student's *t*-test (**l**, **t**) or one-way ANOVA (**n**). $*P < 0.05$; $**P < 0.01$; $***P < 0.001$; $****P < 0.0001$.

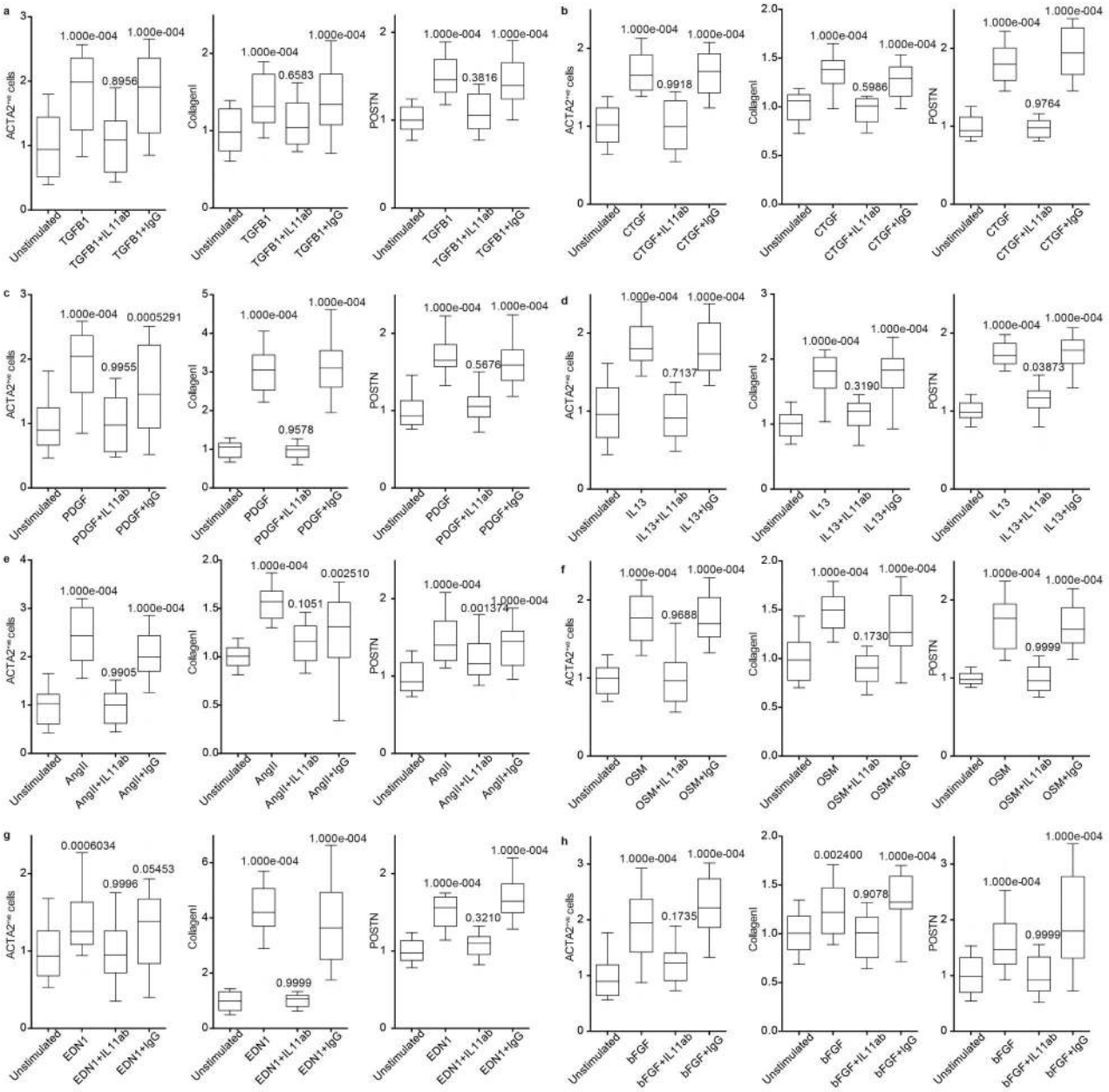

Extended Data Figure 6. IL-11 is required for the pro-fibrotic effects of multiple stimuli

a–**h**, Cardiac fibroblasts were incubated for 24 h with TGFβ1 (**a**; 5 ng ml^{-1}), CTGF (**b**; 50 ng ml^{-1}), PDGF (**c**; 200 ng ml^{-1}), IL-13 (**d**; 100 ng ml^{-1}), AngII (**e**; 100 nM), OSM (**f**; 100 ng ml^{-1}), EDN1 (**g**; 250 ng ml^{-1}) or bFGF (**h**; 10 ng ml^{-1}) in the presence or absence of an IL-11-neutralizing antibody (IL-11ab) or IgG control (2 μg ml^{-1}). Cells were stained for

ACTA2, collagen I and POSTN to monitor the amount of myofibroblasts and ECM production. High-content imaging and quantification of fluorescence (Operetta assay $n = 7$ measurements per $n = 6$ independent experiments for each condition and cellular phenotype) revealed that anti-IL-11 antibodies significantly reduce the pro-fibrotic effect of these stimuli on myofibroblast ratio and ECM production. Two-tailed Dunnett's test. Box-and-whisker plots show median (middle line), 25th–75th percentiles (box) and 10th–90th percentiles (whiskers).

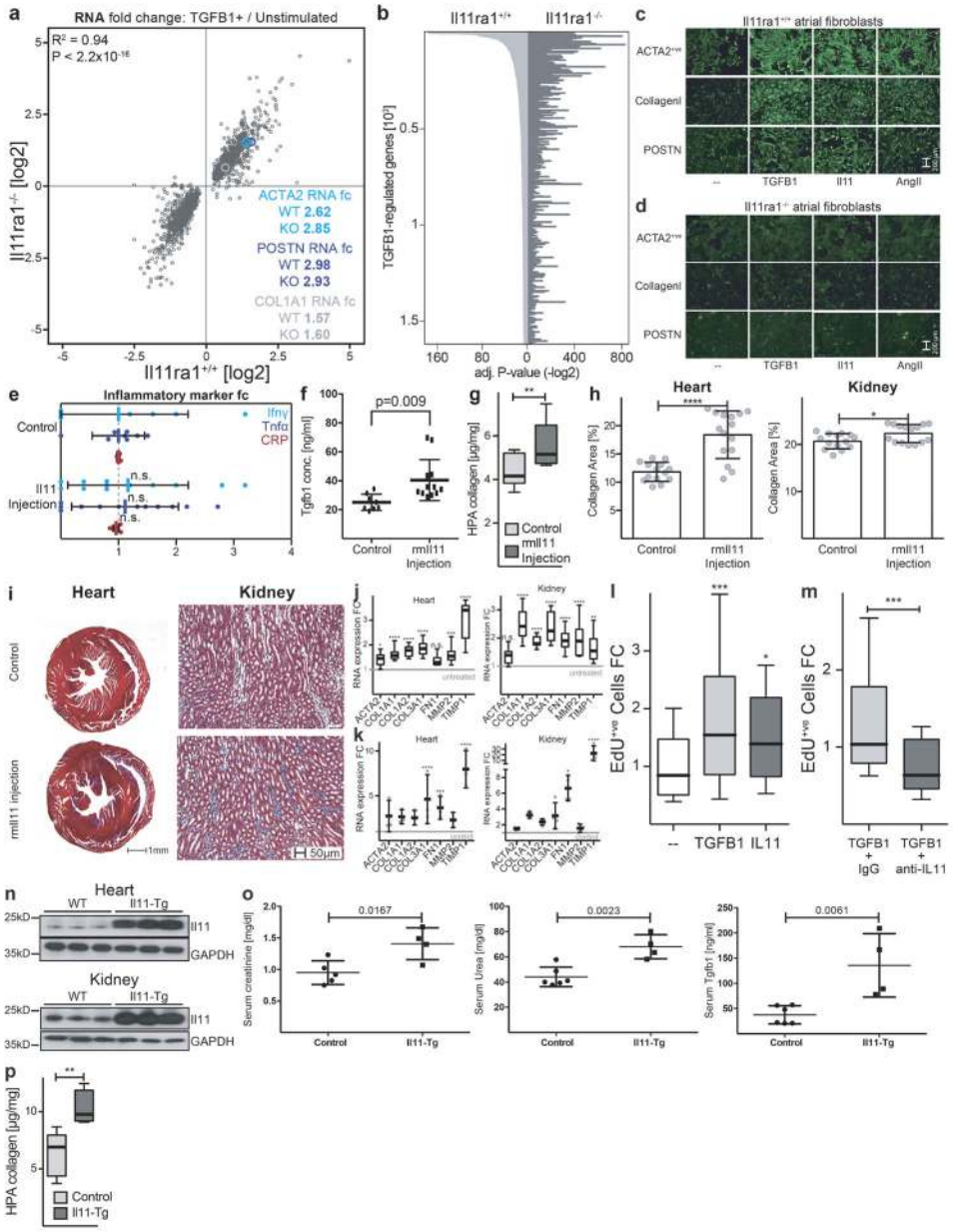

Extended Data Figure 7. Il-11 acts post-transcriptionally and causes fibrosis *in vivo*

a, RNA-seq fold change in TGFβ1-regulated genes in *Il11ra1*$^{+/+}$ cardiac fibroblasts ($n = 3$ biologically independent samples) compared to *Il11ra1*$^{-/-}$ cardiac fibroblasts ($n = 3$

biologically independent samples) after TGFβ1 stimulation (5 ng ml^{-1}, 24 h) are highly correlated. Spearman's correlation shows that RNA levels of fibrosis genes are upregulated equally in both genotypes. **b**, Wild-type and knockout fibroblasts ($n = 3$ biologically independent samples) were incubated with TGFβ1 (5 ng ml^{-1}, 24 h) and RNA-seq was performed to detect differentially expressed genes using DEseq2. All genes regulated by TGFβ1 in wild-type cells are plotted with decreasing $-\log_2(P_{\text{adjusted}})$. The *P* value of the same genes in stimulated *Il11ra1*$^{-/-}$ cells are plotted to the right. A similar *P*-value distribution suggests that TGFβ1-driven RNA expression changes are still present in the absence of IL-11 signalling showing that loss of Il11ra1 does not influence the TGFβ1-driven transcriptional response. **c**, **d**, Primary atrial fibroblasts were prepared from *Il11ra1*$^{+/+}$ (**c**) or *Il11ra1*$^{-/-}$ (**d**) mice were incubated for 24 h without stimulus or with TGFβ1 (5 ng ml^{-1}), IL-11 (5 ng ml^{-1}) or AngII (100 nM). Cells were stained with antibodies against ACTA2, collagen I or POSTN. Images were taken at low magnification (10×) on the Operetta imaging platform. As shown, fibroblasts from knockout mice do not respond to pro-fibrotic stimuli at the level of pro-fibrotic protein expression. This experiment was repeated four times with similar results. **e**, Circulating markers of inflammation after rmIl-11 injection (100 μg kg^{-1} per day, three weeks; $n = 14$ biologically independent samples). **f**, Circulating levels of Tgfβ1 (ELISA) after rmIl-11 injection (control, $n = 8$; Il-11 injection, $n = 12$ biologically independent samples). **g**, Collagen content (HPA assay) in atrium (control, $n = 7$; rmIl-11, $n = 10$ biologically independent samples) after rmIL-11 treatment. **h**, The area indicative for collagen deposition was assessed over several fields in $n = 4$ biologically independent samples and compared between samples from rmIl-11-treated and control mice. **i**, Representative histological images of the heart and kidney after rmIl-11 injection indicate increased collagen content according to Masson's trichrome staining. This experiment was repeated three times with similar results. **j**, RNA expression (RT–qPCR) of fibrosis genes in heart ($n = 12$ biologically independent samples) and kidney ($n = 11$ biologically independent samples) after rmIl-11 treatment compared to control. **k**, RNA expression (RT–qPCR) of fibrosis genes in heart (control, $n = 6$; Il-11-Tg, $n = 3$ biologically independent samples) and kidney (control, $n = 7$; Il-11-Tg, $n = 4$ biologically independent samples) of tamoxifen-treated Il-11-Tg, Col1a2–CreER and control mice. **l**, Cardiac fibroblasts were incubated with TGFβ1 or IL-11 (5 ng ml^{-1}) and EdU (10 μM ml^{-1}, 24 h), which was used to detect replicating DNA by fluorescence by automated quantification of images (Operetta assay $n =$ 7 measurements per $n = 6$ independent experiments). This analysis reveals a significant increase in fibroblast proliferation (EdU^{+} ells) induced by both TGFβ1 and IL-11. The percentage of EdU^{+} cells was normalized to the average detected in non-stimulated cells. **m**, Cells were incubated with TGFβ1 (5 ng ml^{-1}, 24 h) and either an IgG control or anti-IL-11 antibody (2 μg ml^{-1}, 24 h). High-content imaging (Operetta assay $n = 7$ measurements per $n = 6$ independent experiments) and quantification of proliferating cells show that anti-IL-11 antibodies significantly reduce the effects of TGFβ1 on fibroblast proliferation. The percentage of EdU^{+} ells was normalized to the average detected in cells stimulated with TGFβ1 and IgG control. **n**, Western blots show an increase in Il-11 protein expression in the heart and kidney after tamoxifen treatment in Il-11-Tg, Col1a2–CreER mice. **o**, Il-11 transgenic mice were crossed with a Col1a2- promoter, tamoxifen-inducible Cre mouse strain (Il-11-Tg). Six-week-old mice were treated with tamoxifen (1 mg per day, 10 consecutive days) to induce Cre-mediated recombination. Likewise, wild-type littermates

were injected with tamoxifen for 10 consecutive days as controls. The mice (control creatinine, $n = 5$; Il-11-Tg creatinine, $n = 4$; control urea, $n = 6$; Il-11-Tg urea, $n = 4$; control Tgfβ1, $n = 6$; Il-11-Tg Tgfβ1, $n = 4$ biologically independent samples) were euthanized 14 days after cessation of tamoxifen administration. Serum urea and creatinine increased and indicated renal impairment. We also observed an increase in circulating Tgfβ1 levels. **p**, Collagen content (HPA assay) in atrium (control, $n = 11$; Il-11-Tg, $n = 4$ biologically independent samples) from tamoxifentreated or control Il-11-Tg mice. Data are mean ± s.d. (**e**, **f**, **h**, **k**, **o**); box-and-whisker plots (**g**, **j**, **l**, **m**, **p**) show median (middle line), 25th–75th percentiles (box) and 10th–90th percentiles (whiskers). Sidak-corrected, two-tailed Student's *t*-test (**e**, **j**, **k**) or two-tailed Student's *t*-test (**f**–**h**, **m**, **o**, **p**) or Dunnett's test (**l**). $*P < 0.05$; $**P < 0.01$; $***P < 0.001$; $****P < 0.0001$.

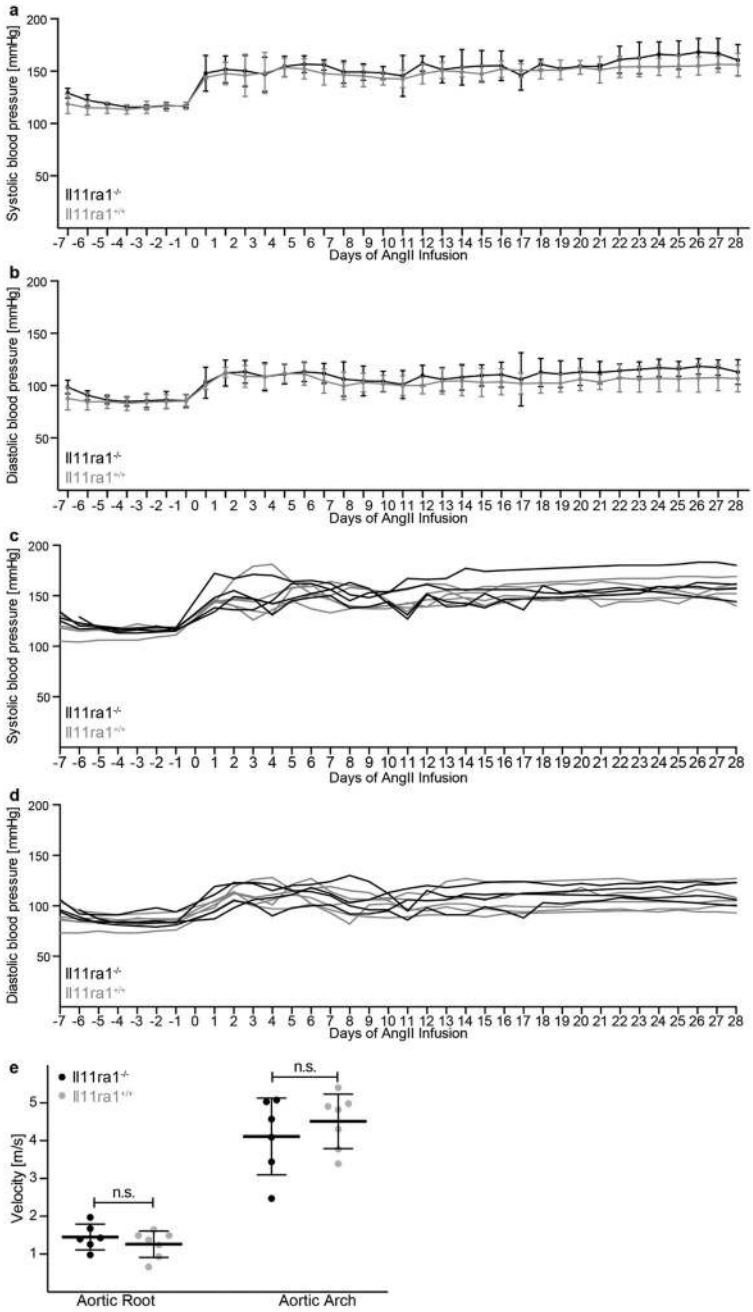

Extended Data Figure 8. Il-11 inhibition does not alter blood pressure after AngII treatment

Il11ra1$^{+/+}$ wild-type ($n = 4$ biologically independent samples) and *Il11ra1*$^{-/-}$ knockout ($n =$ 5 biologically independent samples) mice were injected with AngII (2 mg kg^{-1} per day, 28 days). **a**, **b**, Systolic (**a**) and diastolic (**b**) blood pressure was measured by *in vivo* telemetry for one week before and four weeks after the AngII infusion. Systolic (**c**) and diastolic (**d**) blood pressure for individual mice. AngII resulted in an increase in blood pressure as expected. The genotype did not have a significant effect on blood pressure. **e**, Aortic root or arch velocity of the blood. There was no significant difference in the degree of aortic

constriction in the TAC model between genotypes ($n = 6$ biologically independent samples). Two-sided Mann–Whitney *U*-test (**e**). n.s., not significant. Data are mean ± s.d. (**a**, **b**, **e**).

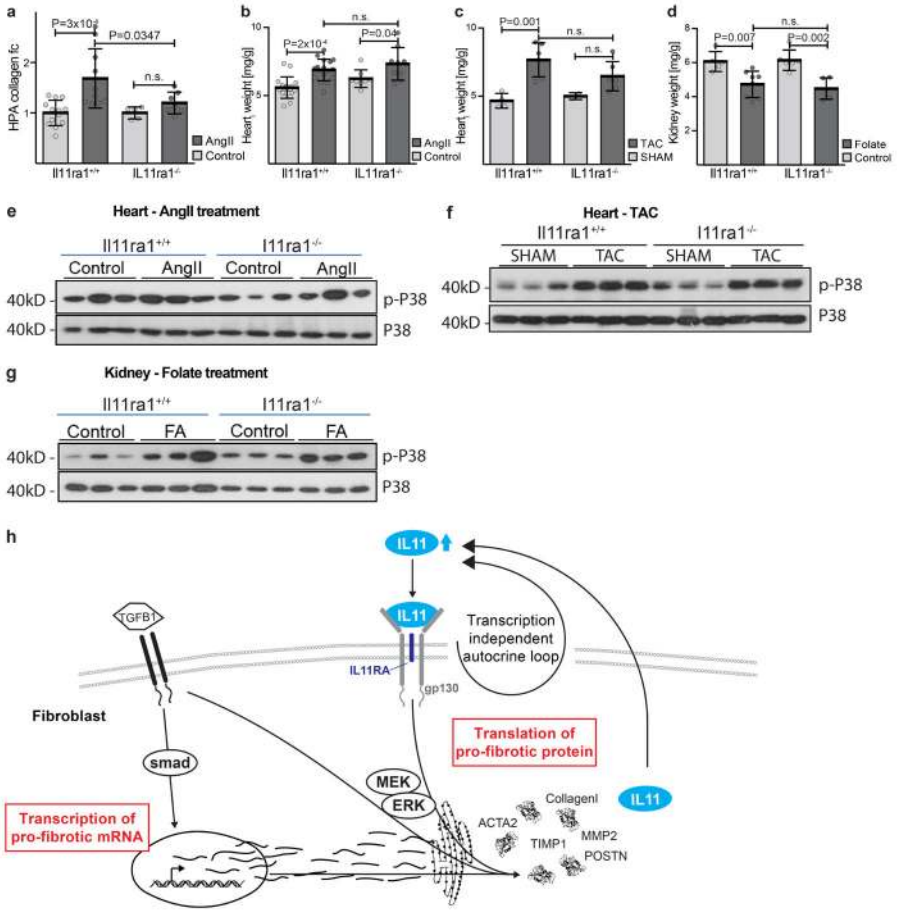

Extended Data Figure 9. Reduction in collagen deposition in *Il11ra1*$^{-/-}$ animals is independent of p38 MAPK signalling

Il11ra1$^{+/+}$ mice (control, $n = 13$; AngII, $n = 10$ biologically independent samples) and *Il11ra1*$^{-/-}$ mice (control, $n = 5$; AngII, $n = 7$ biologically independent samples) were injected with AngII (100 μg kg^{-1} per day, three weeks). **a**, HPA assay of ventricular tissue shows a decrease in collagen deposition in *Il11ra1*$^{-/-}$ mice after AngII infusion. **b**, Indexed heart weight of wild-type (control, $n = 17$; AngII, $n = 17$ biologically independent samples) and *Il11ra1*$^{-/-}$ (control, $n = 8$; AngII, $n = 9$ biologically independent samples) mice after AngII injection. **c**, Indexed heart weight of *Il11ra1*$^{+/+}$ (control, $n = 4$; TAC, $n = 6$ biologically independent samples) and *Il11ra1*$^{-/-}$ (control, $n = 6$; TAC, $n = 6$ biologically independent samples) mice after TAC. **d**, Kidney weight of *Il11ra1*$^{+/+}$ (control, $n = 5$; folate, $n = 8$ biologically independent samples) and *Il11ra1*$^{-/-}$ (control, $n = 6$; folate, $n = 5$ biologically independent samples) mice three weeks after folate injection (180 mg kg^{-1}). **a–d**, Sidak-corrected, two-tailed Student's *t*-test. Data are mean ± s.d. **e–g**, Western blot of p38 MAPK signalling in tissues of *Il11ra1*$^{+/+}$ and *Il11ra1*$^{-/-}$ mice after AngII infusion (e), TAC (f) or folate treatment (**g**). h, Schematic showing the proposed role of IL-11 fibroblasts. An autocrine loop of IL-11 signalling is required to feed-forward changes in pro-fibrotic mRNA

abundances to the protein level by activating translational processes that are ERK-dependent. Blocking this loop limits fibrosis caused by multiple upstream stimuli and fibrosis in preclinical models of heart and kidney disease.

Extended Data Table 1

84 patients undergoing coronary artery bypass grafting donated right atrial biopsies

DEMOGRAPHICS	
Age (years)	60.2 ± 7.2
Sex (M/F)	69/15
Race (CH/MY/IN/other)	53/12/16/3
Height (m)	1.6 ± 0.1
Weight (kg)	70.3 ± 12.0
Waist Circumference (cm)	93.6 ± 11.2
Hip Circumference (cm)	97.0 ± 9.5
Systolic BP (mmHg)	128.5 ± 17.1
Diastolic BP (mmHg)	73.0 ± 9.2
MEDICAL HISTORY	
Hypertension (Y/N)	74/8
Smoking (Y/N/Ex)	12/41/29
Myocardial infarct (Y/N)	33/40
Atrial fibrillation* (Y/N)	5/74
Diabetes (Y/N)	50/34
Diuretic (Y/N)	8/76
Beta Blocker (Y/N)	74/10
Nitrate (Y/N)	52/32
Insulin (Y/N)	13/71
Oral anti-diabetic (Y/N)	42/41
ACE or ARB (Y/N)	46/38
Statin (Y/N)	80/4
Calcium antagonist (Y/N)	26/56
ECG DATA	
PR (ms)	174 ± 29
QRS (ms)	93.8 ± 15.5
QT (ms)	415.5 ± 35.3
Heart rate (bpm)	69.0 ± 11.0
BLOOD TESTS	
Hemoglobin (g/L)	13.6 ± 1.6
Urea (mM/L)	5.7 ± 2.2
Creatinine (μM/L)	101.1 ± 70.1
Fasting glucose (mM/L)	7.9 ± 3.5

ECHO DATA	
LVEF (%)	52.3 ± 12.9
Left atrial area (cm^2)	4.1 ± 0.7
LVIDd (cm)	4.9 ± 0.7
LVIDs (cm)	3.3 ± 0.8
E/A Ratio	1.1 ± 0.7
BIOPSY	
Biopsy weight (mg)	94.6 ± 59.5

Categorical data are presented as yes (Y) or no (N), unless otherwise indicated. Echocardiography (Echo) data: left ventricular ejection fraction (LVEF), left ventricular internal diameter in diastole (LVIDd), left ventricular internal diameter in systole (LVIDs), mitral valve inflow measured as ratio of peak velocity flow in early diastole (E) compared to late diastole (A) caused by atrial contraction (E/A) ratio. Atrial fibrillation* refers to any present or previous history of atrial fibrilation. Quantitative data represented as mean ±s.d. CH, Chinese; Ex, ex-smoker; IN, Indian sub- continent; MY, Malaysian.

Supplementary Material

Refer to Web version on PubMed Central for supplementary material.

Acknowledgments

We thank all patients for taking part in this research, which was performed with approval from the SingHealth Centralised IRB Review Board (CIRB; 2013/103/C). The research was supported by the National Medical Research Council (NMRC) Singapore STaR award (S.A.C.) (NMRC/STaR/0011/2012), the NMRC Centre Grant to the National Heart Centre Singapore (NHCS), Goh Foundation, Tanoto Foundation, NHLBI 5R01HL080494 (J.G.S., C.E.S.), HHMI (C.E.S.) and a grant from the Fondation Leducq (N.H., J.G.S., C.E.S., S.C.). We thank I. Kamer and R. Plehm, Max-Delbrück-Center for Molecular Medicine (MDC), for expert technical help with telemetry blood pressure measurements.

References

1. Rockey DC, Bell PD, Hill JA. Fibrosis—a common pathway to organ injury and failure. N Engl J Med. 2015; 372:1138–1149. [PubMed: 25785971]
2. Burstein B, Nattel S. Atrial fibrosis: mechanisms and clinical relevance in atrial fibrillation. J Am Coll Cardiol. 2008; 51:802–809. [PubMed: 18294563]
3. Leaf IA, Duffield JS. What can target kidney fibrosis? Nephrol Dial Transplant. 2017; 32(suppl 1):i89–i97. [PubMed: 28391346]
4. Davis J, Molkentin JD. Myofibroblasts: trust your heart and let fate decide. J Mol Cell Cardiol. 2014; 70:9–18. [PubMed: 24189039]
5. Akhurst RJ, Hata A. Targeting the TGFβ signalling pathway in disease. Nat Rev Drug Discov. 2012; 11:790–811. [PubMed: 23000686]
6. Bierie B, et al. Abrogation of TGF-β signaling enhances chemokine production and correlates with prognosis in human breast cancer. J Clin Invest. 2009; 119:1571–1582. [PubMed: 19451693]
7. Shull MM, et al. Targeted disruption of the mouse transforming growth factor-β1 gene results in multifocal inflammatory disease. Nature. 1992; 359:693–699. [PubMed: 1436033]
8. Wynn TA. Cellular and molecular mechanisms of fibrosis. J Pathol. 2008; 214:199–210. [PubMed: 18161745]
9. Cucoranu I, et al. NAD(P)H oxidase 4 mediates transforming growth factor-β1- induced differentiation of cardiac fibroblasts into myofibroblasts. Circ Res. 2005; 97:900–907. [PubMed: 16179589]

10. Love MI, Huber W, Anders S. Moderated estimation of fold change and dispersion for RNA-seq data with DESeq2. Genome Biol. 2014; 15:550. [PubMed: 25516281]
11. GTEx Consortium. The Genotype-Tissue Expression (GTEx) project. Nat Genet. 2013; 45:580–585. [PubMed: 23715323]
12. FANTOM Consortium and the RIKEN PMI and CLST (DGT). A promoter-level mammalian expression atlas. Nature. 2014; 507:462–470. [PubMed: 24670764]
13. Schmitt JP, et al. Dilated cardiomyopathy and heart failure caused by a mutation in phospholamban. Science. 2003; 299:1410–1413. [PubMed: 12610310]
14. Du XX, Neben T, Goldman S, Williams DA. Effects of recombinant human interleukin-11 on hematopoietic reconstitution in transplant mice: acceleration of recovery of peripheral blood neutrophils and platelets. Blood. 1993; 81:27–34. [PubMed: 8417798]
15. Putoczki TL, et al. Interleukin-11 is the dominant IL-6 family cytokine during gastrointestinal tumorigenesis and can be targeted therapeutically. Cancer Cell. 2013; 24:257–271. [PubMed: 23948300]
16. Obana M, et al. Therapeutic activation of signal transducer and activator of transcription 3 by interleukin-11 ameliorates cardiac fibrosis after myocardial infarction. Circulation. 2010; 121:684–691. [PubMed: 20100971]
17. Ernst M, Putoczki TL. Molecular pathways: IL11 as a tumor-promoting cytokine—translational implications for cancers. Clin Cancer Res. 2014; 20:5579–5588. [PubMed: 25074610]
18. Lokau J, et al. Proteolytic cleavage governs interleukin-11 *trans*-signaling. Cell Reports. 2016; 14:1761–1773. [PubMed: 26876177]
19. Dams-Kozlowska H, et al. A designer hyper interleukin 11 (H11) is a biologically active cytokine. BMC Biotechnol. 2012; 12:8. [PubMed: 22433466]
20. Nandurkar HH, et al. Adult mice with targeted mutation of the interleukin-11 receptor (IL11Ra) display normal hematopoiesis. Blood. 1997; 90:2148–2159. [PubMed: 9310465]
21. Duan J, et al. Wnt1/β catenin injury response activates the epicardium and cardiac fibroblasts to promote cardiac repair. EMBO J. 2012; 31:429–442. [PubMed: 22085926]
22. Kaye JA. FDA licensure of NEUMEGA to prevent severe chemotherapyinduced thrombocytopenia. Stem Cells. 1998; 16(Suppl 2):207–223. [PubMed: 11012193]
23. Moore-Morris T, et al. Resident fibroblast lineages mediate pressure overload-induced cardiac fibrosis. J Clin Invest. 2014; 124:2921–2934. [PubMed: 24937432]
24. Paul SR, et al. Molecular cloning of a cDNA encoding interleukin 11, a stromal cell-derived lymphopoietic and hematopoietic cytokine. Proc Natl Acad Sci USA. 1990; 87:7512–7516. [PubMed: 2145578]
25. Nakagawa M, et al. Four cases of investigational therapy with interleukin-11 against acute myocardial infarction. Heart Vessels. 2016; 31:1574–1578. [PubMed: 26796134]
26. Lindahl GE, et al. Microarray profiling reveals suppressed interferon stimulated gene program in fibroblasts from scleroderma-associated interstitial lung disease. Respir Res. 2013; 14:80. [PubMed: 23915349]
27. Nieminen P, et al. Inactivation of IL11 signaling causes craniosynostosis, delayed tooth eruption, and supernumerary teeth. Am J Hum Genet. 2011; 89:67–81. [PubMed: 21741611]
28. Satija R, Farrell JA, Gennert D, Schier AF, Regev A. Spatial reconstruction of single-cell gene expression data. Nat Biotechnol. 2015; 33:495–502. [PubMed: 25867923]
29. Trapnell C, Pachter L, Salzberg SL. TopHat: discovering splice junctions with RNA-seq. Bioinformatics. 2009; 25:1105–1111. [PubMed: 19289445]
30. Anders S, Pyl PT, Huber W. HTSeq—a Python framework to work with high-throughput sequencing data. Bioinformatics. 2015; 31:166–169. [PubMed: 25260700]
31. Subramanian A, et al. Gene set enrichment analysis: a knowledge-based approach for interpreting genome-wide expression profiles. Proc Natl Acad Sci USA. 2005; 102:15545–15550. [PubMed: 16199517]
32. Langfelder P, Horvath S. WGCNA: an R package for weighted correlation network analysis. BMC Bioinformatics. 2008; 9:559. [PubMed: 19114008]

33. Bolger AM, Lohse M, Usadel B. Trimmomatic: a flexible trimmer for Illumina sequence data. Bioinformatics. 2014; 30:2114–2120. [PubMed: 24695404]
34. Babraham Bioinformatics. FastQC, a quality control tool for high throughput sequence data. http://www.bioinformatics.babraham.ac.uk/projects/fastqc/
35. Dobin A, et al. STAR: ultrafast universal RNA-seq aligner. Bioinformatics. 2013; 29:15–21. [PubMed: 23104886]
36. Liao Y, Smyth GK, Shi W. featureCounts: an efficient general purpose program for assigning sequence reads to genomic features. Bioinformatics. 2014; 30:923–930. [PubMed: 24227677]
37. Burke MA, et al. Molecular profiling of dilated cardiomyopathy that progresses to heart failure. JCI Insight. 2016; 1:e86898. [PubMed: 27239561]
38. Tarnavski O, et al. Mouse cardiac surgery: comprehensive techniques for the generation of mouse models of human diseases and their application for genomic studies. Physiol Genomics. 2004; 16:349–360. [PubMed: 14679301]
39. Zheng B, Zhang Z, Black CM, de Crombrugghe B, Denton CP. Ligand-dependent genetic recombination in fibroblasts: a potentially powerful technique for investigating gene function in fibrosis. Am J Pathol. 2002; 160:1609–1617. [PubMed: 12000713]
40. Ye L, et al. Thymosin β 4 increases the potency of transplanted mesenchymal stem cells for myocardial repair. Circulation. 2013; 128(Suppl 1):S32–S41. [PubMed: 24030419]
41. Gao S, Ho D, Vatner DE, Vatner SF. Echocardiography in mice. Curr Protoc Mouse Biol. 2011; 1:71–83. [PubMed: 21743841]
42. Tortoledo FA, Quinones MA, Fernandez GC, Waggoner AD, Winters WL Jr. Quantification of left ventricular volumes by two-dimensional echocardiography: a simplified and accurate approach. Circulation. 1983; 67:579–584. [PubMed: 6821900]
43. Mead TJ, Lefebvre V. Proliferation assays (BrdU and EdU) on skeletal tissue sections. Methods Mol Biol. 2014; 1130:233–243. [PubMed: 24482177]

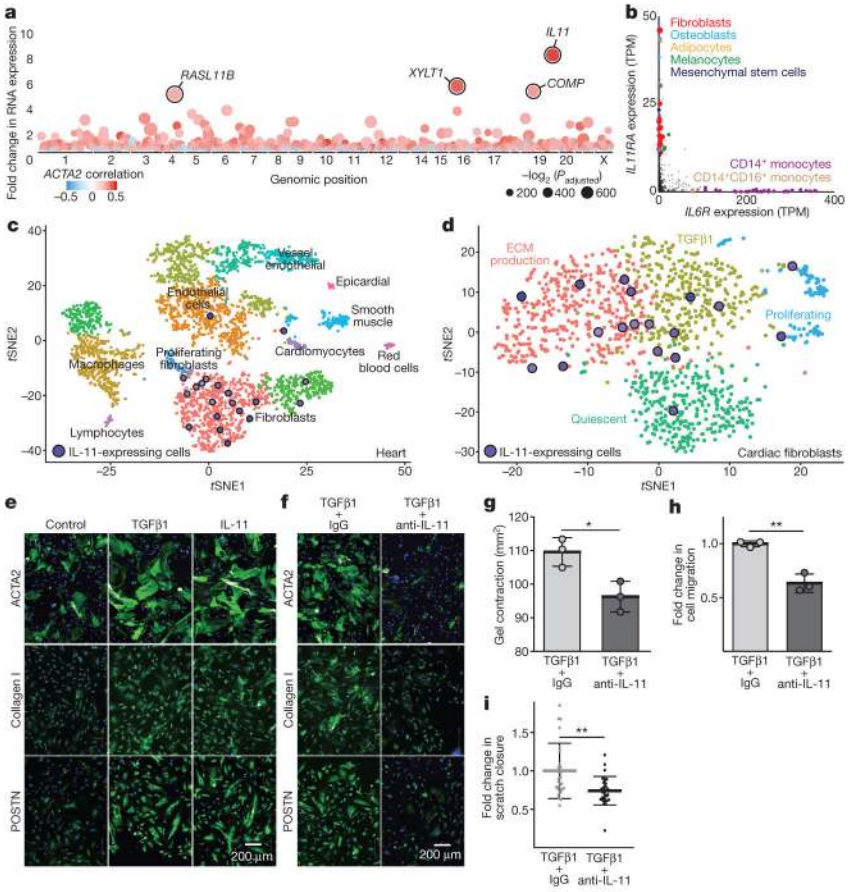

Figure 1. Fibrosis target discovery platform identifies IL-11

a, RNA-seq of primary cardiac fibroblasts ($n = 84$ biologically independent samples) with or without TGFβ1 treatment (5 ng ml^{-1}, 24 h) and Spearman's correlation of expression changes with fibroblast activation (Supplementary Table 2). DEseq2[10] fold change in expression and false-discovery rate (FDR)-adjusted *P* values are shown. **b**, RNA expression in transcripts per million (TPM) of *IL11RA* and *IL6R* across 512 cell lines from the FANTOM repository[12]. **c**, Single-cell resolution of cardiac *Il11* expression (more than 0 reads per cell). *t*-distributed stochastic neighbour embedding (*t*SNE) analysis[28] clusters cell types of the heart. *Il11* expression is highly enriched in fibroblasts. χ^2 test ($P = 5.7 \times 10^{-8}$). **d**, *t*SNE analysis of fibroblasts alone shows highest Il-11 expression in ECM-secreting and TGFβ1-activated fibroblasts. χ^2 test ($P = 0.033$). **c**, **d**, Cardiac cells were sequenced from $n = 1$ mouse, the experiment was repeated once with similar results. **e**, **f**, Representative images (chosen from 42 per condition) of cardiac fibroblasts immunostained for ACTA2, collagen I or periostin (POSTN) after a 24-h incubation without stimulus (control), TGFβ1 or IL-11 (5 ng ml^{-1}) (**e**) or with TGFβ1 (5 ng ml^{-1}) and an anti-IL-11 neutralizing antibody or an IgG control (2 μg ml^{-1}) (**f**). **g**, Cardiac fibroblasts were seeded in collagen gel and the area of contraction determined ($n = 3$ biologically independent samples) after 72 h. **h**, Trans-well migration assay (colourimetrically quantified, $n = 3$ biologically independent samples, 24 h). **i**, Scratch assay of wound closure in a monolayer of cardiac fibroblasts ($n = 5$

biologically independent samples) after 24 h. **g–i**, Two-tailed Student's *t*-test; data are mean ± s.d.; **P* < 0.05; ***P* < 0.01.

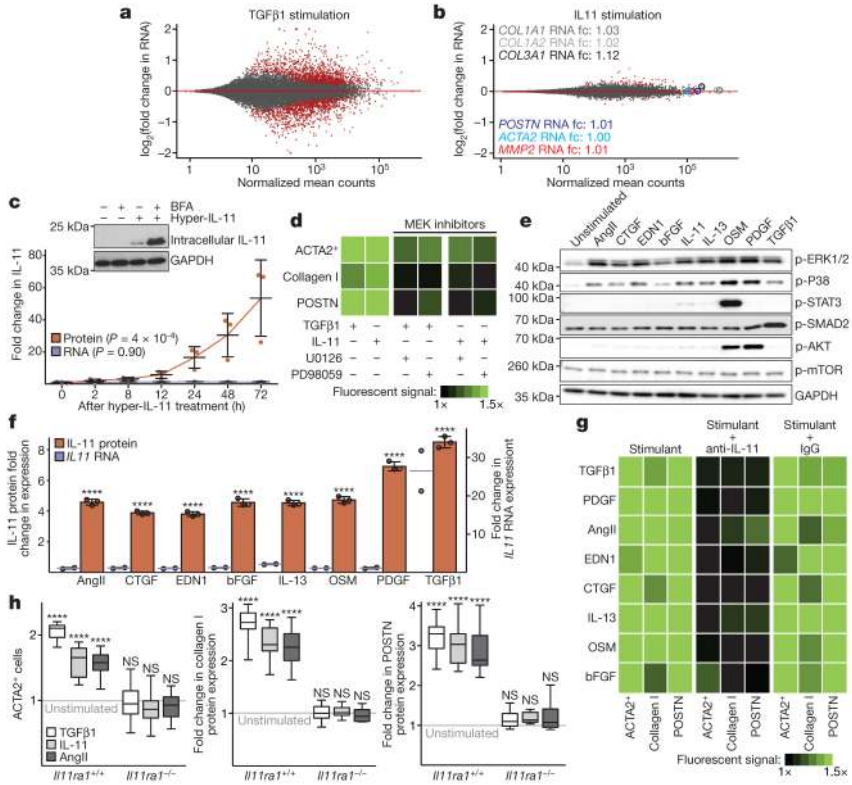

Figure 2. Non-canonical IL-11 signalling drives fibrogenic protein synthesis

a, **b**, RNA-seq of primary cardiac fibroblasts in response to TGFβ1 (**a**) or IL-11 (**b**) ($n = 6$ biologically independent samples, 5 ng ml^{-1}, 24 h). Red indicates significantly differentially expressed genes (FDR ≤0.05, DEseq2[10]). RNA expression of genes associated with fibrosis is not increased by IL-11 treatment. fc, fold change. **c**, ELISA and quantitative PCR with reverse transcription (RT–qPCR) assays of IL-11 expression ($n = 3$ biologically independent samples) after hyperIL-11 treatment (0.2 ng ml^{-1}). Benjamini–Hochberg corrected one-way ANOVA; data are mean ± s.d. Inset, western blot of cardiac fibroblast lysates after hyperIL-11 stimulation and brefeldin A (BFA, 1 μg ml^{-1}) treatment indicates canonical secretion of IL-11. **d**, Cardiac fibroblasts were incubated with TGFβ1, IL-11 (5 ng ml^{-1}) and MEK inhibitors U0126 or PD98059 (10 μM, 24 h). ACTA2^{+} cells and ECM production was assessed and normalized to non-stimulated cells. **e**, Western blots of phosphorylated protein (p-) expression of signalling pathways in cardiac fibroblasts in response to various pro-fibrotic stimuli (see also Extended Data Fig. 5). **f**, ELISA (supernatant, $n = 3$ biologically independent samples) and RT–qPCR ($n = 2$ biologically independent samples) of IL-11 expression in cardiac fibroblasts after 24 h stimulation with AngII (100 nM), CTGF (50 ng ml^{-1}), EDN1 (250 ng ml^{-1}), bFGF (10 ng ml^{-1}), IL-13 (100 ng ml^{-1}), OSM (100 ng ml^{-1}), PDGF (200 ng ml^{-1}) and TGFβ1 (5 ng ml^{-1}). Two-tailed Dunnett's test; Data are mean ± s.d. **g**, Cardiac fibroblasts were incubated with pro-fibrotic cytokines (24 h) and cardiac fibroblast activation was reduced by anti-IL-11 antibodies (2 μg ml^{-1}; Extended Data Fig. 6). **h**, Pro-fibrotic proteins (Operetta assay $n = 7$ measurements per $n = 2$ independent experiments) are not upregulated in cardiac fibroblasts from *Il11ra1*$^{-/-}$ mice in response to TGFβ1, IL-11 (5 ng ml^{-1}) or AngII (100 nM, 24 h). Experiments were repeated twice with

similar results. Two-tailed Dunnett's test; box-and-whisker plots show median (middle line), 25th–75th percentiles (box) and 10th–90th percentiles (whiskers); **** $P < 0.0001$; NS, not significant.

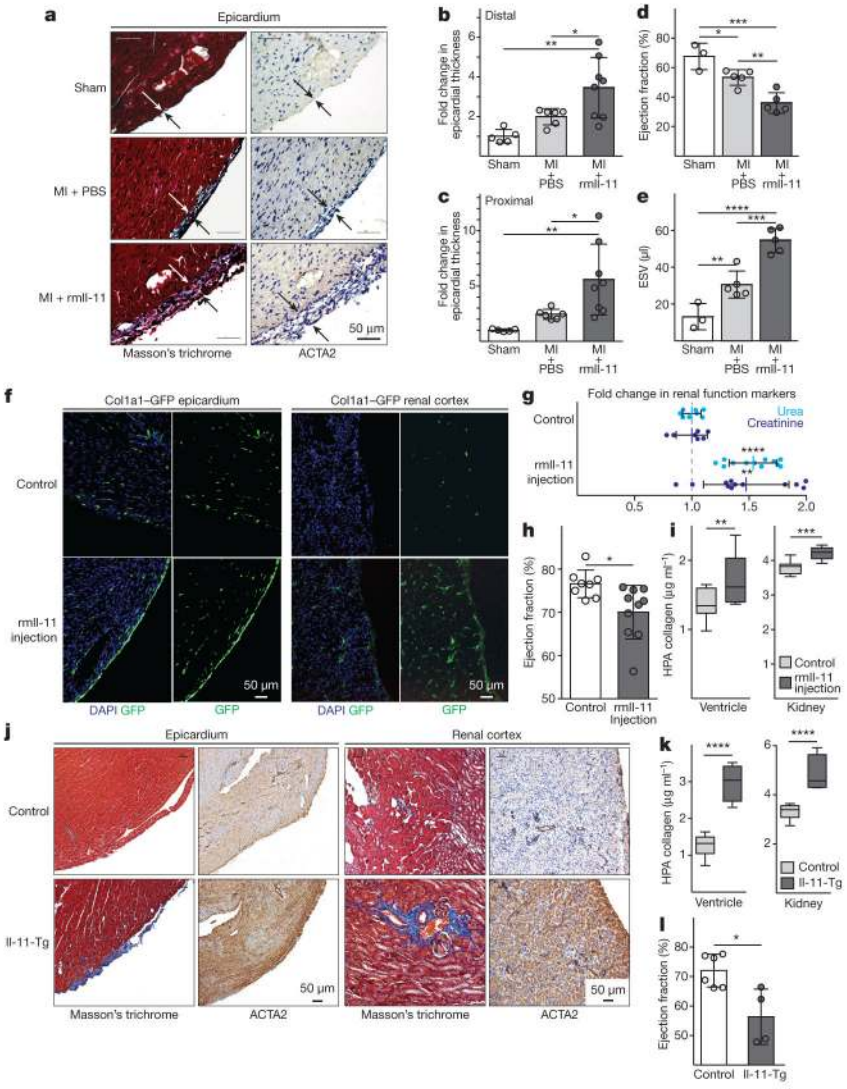

Figure 3. Il-11 causes cardiovascular fibrosis and organ failure

a, Representative histological images of the epicardium with Masson's trichrome staining and ACTA2 immunostaining in mice with myocardial infarction (MI) treated with rmIL-11 or PBS. **b**, **c**, Epicardial thickness of regions distal (**b**) or proximal (**c**) to the region of myocardial infarction. **a**–**c**, Sham, $n = 5$; myocardial infarction, $n = 6$; myocardial infarction + rmIl-11, $n = 8$ biologically independent samples. **d**, **e**, Echocardiography show a decrease in ejection fraction (**d**) and increase in end-systolic volume (ESV) (**e**) after myocardial infarction and rmIl-11 treatment (sham, $n = 3$; myocardial infarction, myocardial infarction + rmIl-11, $n = 5$ biologically independent samples). **b**–**e**, two-tailed, Holm–Sidak-corrected Student's *t*-test; Data are mean ± s.d. **f**, Representative histological images (chosen from control, $n = 3$; rmIl-11 injection, $n = 4$ biologically independent samples) of tissues from a Col1a1–GFP-reporter mouse after rmIL-11 injection (100 µg kg^{-1} per day, three weeks). **g**, Serum urea and creatinine levels after rmIL-11 injection (control urea, $n = 8$; control creatinine, $n = 7$; rmIl-11, $n = 12$ biologically independent samples). **h**, Reduced ejection fraction (echocardiography) in rmIl-11-treated mice. **i**, Hydroxyproline assay (HPA)

quantifies cardiac and renal collagen content after rmIL-11 treatment. **h**, **i**, Control, $n = 8$; rmIl-11, $n = 11$ biologically independent samples. **j**, Representative histological images of Masson's trichrome staining and ACTA2 immunostaining in the epicardium Il-11-Tg mice. **k**, HPA indicates cardiac and renal collagen content in Il-11-Tg mice. **j**, **k**, Control, $n = 12$; Il-11-Tg, $n = 4$ biologically independent samples. **i**, **k**, Two-tailed Student's *t*-test; box-and-whisker plots show median (middle line), 25th–75th percentiles (box) and 10th–90th percentiles (whiskers). **l**, Reduction in ejection fraction (echocardiography) in Il-11-Tg mice (control, $n = 6$; Il-11-Tg, $n = 4$ biologically independent samples). **g**, **h**, **l**, Two-tailed Student's *t*-test; data are mean ± s.d.; $^{*}P < 0.05$; $^{**}P < 0.01$; $^{***}P < 0.001$; $^{****}P < 0.0001$.

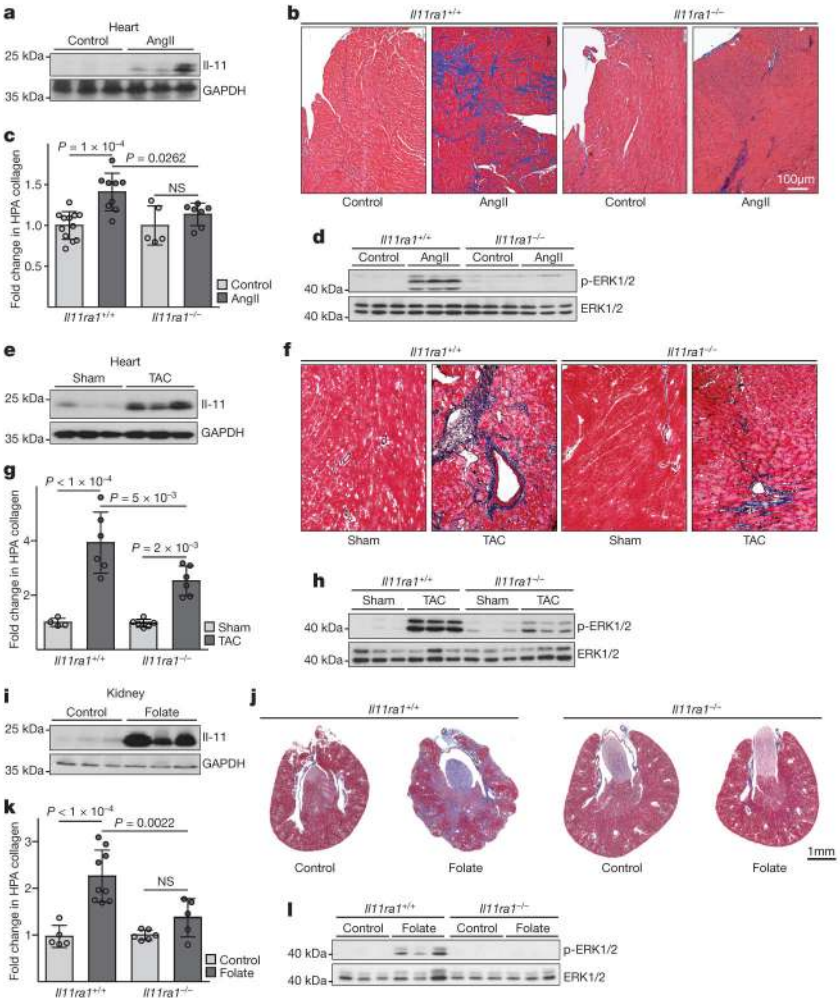

Figure 4. Inhibition of Il-11 reduces cardiovascular fibrosis

a, Western blot of cardiac Il-11 after AngII infusion (2 mg kg^{-1} per day for 28 days). **b**, **c**, Representative histological images (**b**; Masson's trichrome staining) and collagen content (**c**) in the atrium of *Il11ra1*$^{+/+}$ (control, $n = 12$; AngII, $n = 9$ biologically independent samples) and *Il11ra1*$^{-/-}$ (control, $n = 5$; AngII, $n = 7$ biologically independent samples) mice. **d**, Western blot of cardiac ERK activation after AngII infusion. **e**, Western blot of cardiac Il-11 after transverse aortic constriction (TAC). **f**, **g**, Representative histological images (**f**; Masson's trichrome staining) and collagen content. **g**; HPA of hearts from *Il11ra1*$^{+/+}$ (control, $n = 4$; TAC: $n = 6$ biologically independent samples) and *Il11ra1*$^{-/-}$ (control, $n = 6$; TAC, $n = 6$ biologically independent samples) mice after TAC or sham operations. **h**, Western blot of cardiac ERK activation after TAC. **i**, Western blot of renal Il-11 after folate treatment (180 mg kg^{-1}). **j**, **k**, Representative histological images (**j**; Masson's trichrome staining) and collagen content (**k**; HPA assay) of kidneys from *Il11ra1*$^{+/+}$ (control, $n = 5$; folate, $n = 9$ biologically independent samples) and *Il11ra1*$^{-/-}$ (control, $n = 6$; folate, $n = 5$ biologically independent samples) mice. **c**, **g**, **k**, Two-tailed, Sidak-corrected Student's *t*-test;

data are mean ± s.d. NS, not significant. **l**, Western blot of renal ERK activation after folate treatment.